

White dwarf and subdwarf stars in the Sloan Digital Sky Survey Data Release 16

S. O. Kepler¹*, Detlev Koester², Ingrid Pelisoli³, Alejandra D. Romero¹, Gustavo Ourique¹

¹*Instituto de Física, Universidade Federal do Rio Grande do Sul, 91501-900 Porto-Alegre, RS, Brazil*

²*Institut für Theoretische Physik und Astrophysik, Universität Kiel, 24098 Kiel, Germany*

³*Department of Physics, University of Warwick, Gibbet Hill Road, Coventry, CV4 7AL, UK*

Accepted Received 2021 June 15

ABSTRACT

White dwarfs are the end state of the evolution of more than 97% of all stars, and therefore carry information on the structure and evolution of the Galaxy through their luminosity function and initial-to-final mass relation. Examining the new spectra of all white or blue stars in the Sloan Digital Sky Survey Data Release 16, we report the spectral classification of 2410 stars, down to our identification cut-off of signal-to-noise ratio equal to three. We newly identify 1404 DAs, 189 DZs, 103 DCs, 12 DBs, and 9 CVs. The remaining objects are a mix of carbon or L stars (dC/L), narrow-lined hydrogen-dominated stars (sdA), dwarf F stars and P Cyg objects. As white dwarf stars were not targeted by SDSS DR16, the number of new discoveries is much smaller than in previous releases. We also report atmospheric parameters and masses for a subset consisting of 555 new DAs, 10 new DBs, and 85 DZs for spectra with signal-to-noise ratio larger than 10.

Key words: white dwarfs – subdwarfs – catalogues

1 INTRODUCTION

White dwarf stars are the final stage of evolution for all stars formed with initial masses below around $7\text{--}11 M_{\odot}$, depending on metallicity (e.g. Ibeling & Heger 2013; Doherty et al. 2015; Woosley & Heger 2015; Williams et al. 2018; Lauffer et al. 2018), which represent more than 97% of all stars in our Galaxy. White dwarf stars have masses below the Chandrasekhar limit, around $1.4 M_{\odot}$ (e.g. Chandrasekhar 1931; Chandrasekhar & Tooper 1964; Kilic et al. 2021), and their mean mass is around $0.6 M_{\odot}$ (e.g. Koester, Schulz, & Weidemann 1979; Tremblay et al. 2020). They are also possible outcomes of the evolution of multiple systems, with 25–30 per cent of white dwarfs estimated to be the result of mergers (e.g. Toonen et al. 2017). White dwarfs with masses lower than $0.3\text{--}0.45 M_{\odot}$ are generally explained as the result of close binary evolution (e.g. Marsh, Dhillon & Duck 1995; Kilic, Stanek & Pinsonneault 2007), because single progenitors of such low-mass white dwarfs have main sequence lifetimes exceeding the age of the Universe. The formation mechanism of the so-called extremely-low mass white dwarfs (ELMs) – those with masses below $\simeq 0.2\text{--}0.3 M_{\odot}$ (e.g. Sun & Arras 2018; Calcaferro, Althaus, & Córscico 2018, and references therein) – is similar to that proposed to explain hot subdwarf stars (e.g. Heber 2016): the outer envelope is lost after a common envelope or a stable Roche-lobe overflow phase, leaving the stellar core exposed (e.g. Li et al. 2019).

White dwarfs do not present ongoing core nuclear burning, even though residual shell burning may occur depending on the thickness of their outer hydrogen layer. ELM models suggest that they present residual burning before reaching the final white dwarf cooling track (Córscico et al. 2012; Istrate et al. 2016). This happens in the pre-ELM phase (Maxted et al. 2014a,b), which can cause them to brighten to luminosities comparable to main sequence and even horizontal branch stars (e.g. Pietrzynski et al. 2012).

Around 80% of all white dwarfs show solely hydrogen lines, and are classified as spectral class DA. This occurs because the timescales for gravitational settling are of the order of a few million years or smaller (Schatzman 1958; Michaud, Alecian, & Richer 2015), leading to a generally simple atmospheric composition, with the lightest element available on the surface, except for effective temperatures above $\sim 50\,000$ K. The spectral class of the majority remaining is DB, if only He I lines are present, and DO if He II lines are visible — typically with $T_{\text{eff}} \gtrsim 40\,000$ K. Very cool white dwarfs — $T_{\text{eff}} \lesssim 5\,000$ K for H atmosphere, $T_{\text{eff}} \lesssim 11\,000$ K for He atmosphere — show featureless spectra and are classified as DCs. A substantial fraction (20–50 per cent, Zuckerman et al. 2003; Koester, Gänsicke, & Farihi 2014; Hollands et al. 2017; Hollands, Gänsicke, & Koester 2018) of white dwarfs show contamination by metals, which can only be explained by ongoing accretion, except for very hot objects ($T_{\text{eff}} \gtrsim 50\,000$ K), where radiative levitation can still play a significant role (e.g. Bruhweiler & Kondo 1983; Chayer et al. 1989; Barstow et al. 2014); a Z is added to the spectral classification to flag metal pollution. In rare cases, for stars classified

* kepler@if.ufrgs.br

2 *Kepler et al.*

as DQs, carbon may be dragged to the surface by convection (e.g. Koester, Weidemann, & Zeidler 1982; Pelletier et al. 1986; Blouin & Dufour 2019). Cool DQs show spectra similar to dwarf carbon (dC) stars, which are themselves believed to be one outcome of binary evolution (e.g. Whitehouse et al. 2018). Even rarer are those white dwarfs with spectra dominated by oxygen lines, classified as DS (Williams, Kepler, & Sion 2019).

In this paper we extend the work of Kleinman et al. (2013) and Kepler et al. (2015, 2016, 2019), continuing the search for new spectroscopically confirmed white dwarf and subdwarf stars in the data release 16 of the Sloan Digital Sky Survey (SDSS) (SDSS DR16, Ahumada et al. 2020), which contains SDSS observations through August 2018. Spectroscopy allows estimations of T_{eff} , $\log g$, and abundances, serving as a valuable resource for studying stellar formation and evolution in the Milky Way (e.g. Winget et al. 1987; Bergeron, Saffer, & Liebert 1992; Tremblay et al. 2014). As a by-product, we also identify cataclysmic variables (CVs) — white dwarfs with ongoing mass exchange from a companion, and presenting emission lines, generally of hydrogen and helium — and dC stars, due to their spectral similarity with carbon-rich white dwarfs. These dC stars (?), as well as hot subdwarfs and ELMs, hold potential to shed light on the poorly understood process of close binary evolution.

2 DATA ANALYSIS

2.1 Identification of the candidates

This paper follows on the search for new spectroscopically identified white dwarf stars from spectra obtained by the Sloan Digital Sky Survey (Eisenstein et al. 2006; Kleinman et al. 2013; Kepler et al. 2015, 2016, 2019). We started with all the optical spectra obtained after the SDSS Data Release 14. We selected all newly observed spectra within the colour selection of Kleinman et al. (2013), $\approx 78\,000$, and all spectra classified by the SDSS spectral pipeline as WHITE_DWARF, A, B, OB or O stars, or CV (cataclysmic variables), 49 667 spectra. There is partial overlap between the two samples. In addition, we performed an automated algorithm search for spectra similar to previously selected DA and DB training samples, as described in Kepler et al. (2015, 2016, 2019), on all the $\approx 1\,970\,000$ new optical spectra from DR16, which include the sample of already selected spectra. This resulted in the selection of 858 further spectra that were not included in the colour or pipeline classification samples. As white dwarfs were not specifically targeted by DR16, the number of new white dwarfs is smaller than in the previous data releases. Due to the overlaps, we examined these $\approx 128\,000$ selected spectra by eye, to identify broad line spectra characteristic of white dwarfs, hot subdwarfs, and dCs. Using an identification cut-off of $(S/N)_g \geq 3$, where $(S/N)_g$ is the signal-to-noise parameter in the g-band from the SDSS spectra reduction pipeline, we identified 2410 spectra containing white dwarf, subdwarf, CV and dC stars. In Fig. 1 we display three spectra with $(S/N)_g = 70, 13$, and 3, for comparison of the range of S/N we classified. The redder dC/L stars, and some DZs, do not reach $(S/N)_g \geq 3$, but show significant flux at redder wavelengths. As in previous Data Releases, our visual inspection showed that most objects with SDSS spectra, proper motion smaller than 30 mas/yr, and magnitude $g > 20$ are in fact galaxies, from their composite spectrum, high red-shifted lines, or broad emission lines.

2.2 Spectral Classification

DR16 uses improved flux-calibration, with atmospheric differential refraction corrected on a per-exposure basis following the recipe described in Margala et al. (2016), and improved co-addition of individual exposures. The Stellar Parameters Pipeline, which we used in our initial spectral class selection, are from Lee et al. (2008a,b) and Allende Prieto et al. (2008).

The wavelength coverage is from 3650 to 10 400 Å for the BOSS spectrograph, with a resolution of 1500 at 3800 Å and 2500 at 9000 Å, and a wavelength calibration better than 5 km/s. All the spectra used in our analysis were processed with the spectroscopic reduction pipeline version v5_13_0. These RUN2D numbers denote the version of extraction and redshift-finding code used. In all SDSS spectral line descriptions, vacuum wavelengths are used. The wavelengths are shifted such that measured velocities are relative to the solar system barycentre at the mid-point of each 15-minute exposure.

We were conservative in labelling a spectrum as a clean DA or DB, considering we are interested in obtaining accurate mass distributions for our DA and DB stars. We therefore add additional subtypes and uncertainty notations (: if we saw signs of other elements, unresolved companions, or magnetic fields (H) in the spectra. While some of our mixed white dwarf subtypes would possibly be identified as clean DAs or DBs with better signal-to-noise spectra, few of our identified clean DAs or DBs would likely be found to have additional spectral features within our detection limit.

We looked for the following features to aid in the classification for each specified white dwarf subtype:

- Balmer lines — normally broad and with a Balmer decrement [DA but also DAB, DBA, DZA, and subdwarfs]
- HeI 4 471Å [DB, sdB]
- HeII 4 686Å [DO, PG1159, sdO]
- C2 Swan band or atomic CI lines [DQ]
- CII 4 367Å [HotDQ]
- CaII H & K [DZ, DAZ, DBZ]
- Zeeman splitting [magnetic white dwarfs]
- featureless spectrum with significant proper motion [DC]

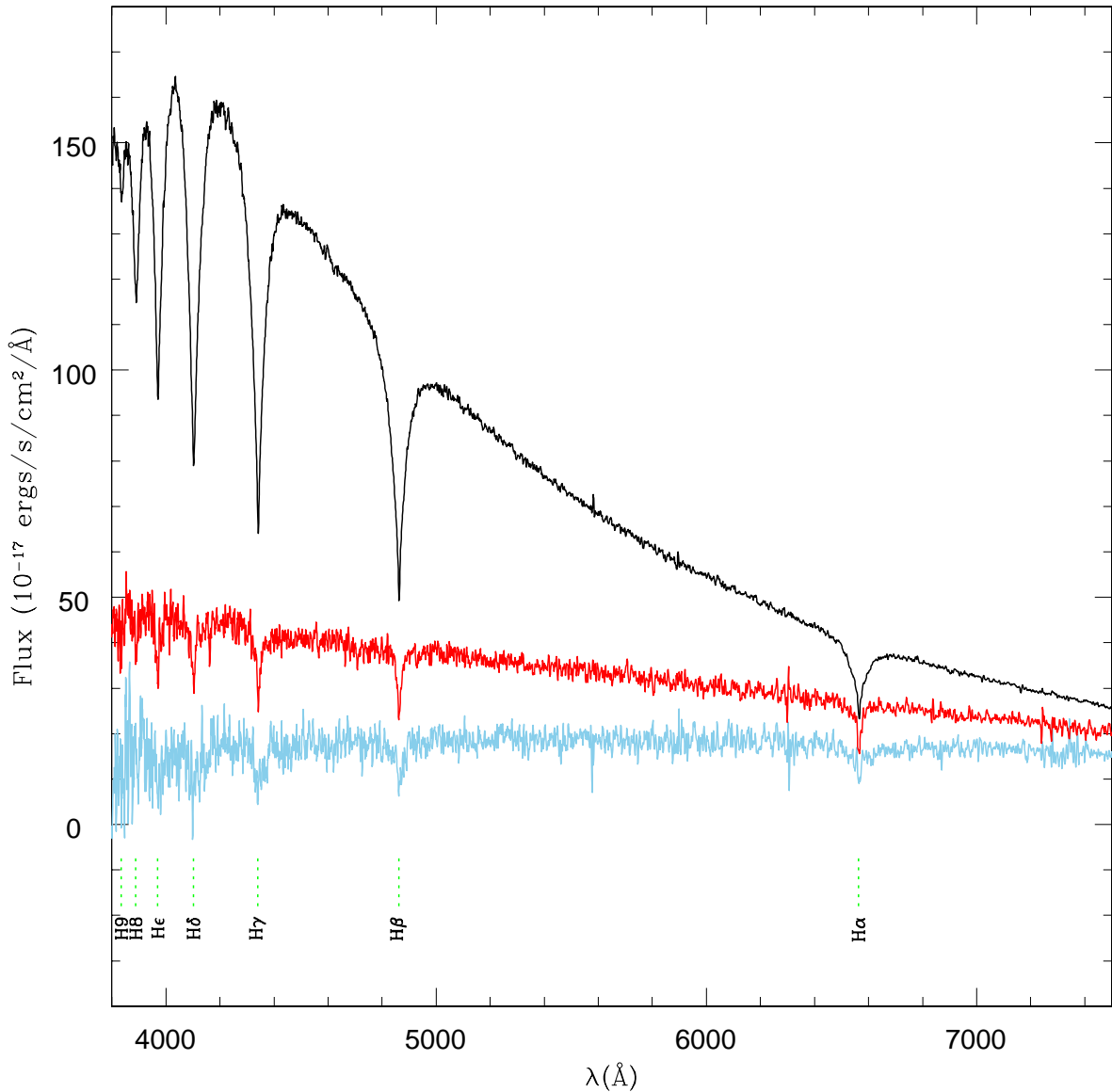


Figure 1. Spectra of three DAs, from top to bottom, $S/N_g=70$, SDSSJ075144.06+223004.80, P-M-F 11112-58428-0632, $g=16.639$; $S/N_g=13$, the mean S/N , SDSS J142707.81+381640.81, P-M-F 10752-58488-0162, $g=18.919$, scaled for display, and $S/N_g=3$, SDSS J132411.33+340028.76, P-M-F 10254-58514-0076, $g=18.319$, scaled, to show the range of S/N we classified.

Table 1. Classification of 2410 spectra in Table 2, including 30 known CVs and one new CV with two spectra.

Number	Type
1404	DA
12	DB
103	DC
189	DZ
41	CV
301	dC/L
320	sdA
16	F
4	P Cyg
1	binary

Table 2. Spectral classification for 2410 white dwarfs and subdwarfs in SDSS DR16. The complete table is available electronically (dr16tabedr3.csv).

SDSS J	Plate-MJD-Fiber	S/N _g	u	σ_u	g	σ_g	r	σ_r	i	σ_i	z	σ_z	E(B-V)	ppm	ℓ	b	DR2par	σ_π	EDR3par	σ_π	ppm _G	G	BP-RP	Type	
			(mag)	(mag)	(mag)	(mas/yr)	(deg)	(deg)	(mas)	(mas)	(mas)	(mas/yr)	(mag)	(mag)											
000007.28+074944.83	11279-58449-0954	06	20.938	0.095	20.481	0.025	20.743	0.036	20.911	0.064	21.306	0.325	0.043	000.0	101.5	-52.9	2.663	1.168	2.866	0.989	30	20.627	0.384	DA	
000035.47+084315.04	11277-58450-0316	06	21.335	0.151	21.422	0.051	21.208	0.059	21.466	0.132	20.497	0.239	0.051	005.4	102.2	-52.1	0.547	0.822	0.339	0.624	02	20.150	0.526	DA	
000035.59-001115.94	09403-58018-0465	07	23.039	0.347	20.271	0.031	18.813	0.017	18.334	0.026	18.118	0.039	0.030	065.8	096.5	-60.4	0.644	0.378	1.403	0.383	64	18.834	1.753	dC	
000155.08+101323.36	11277-58450-0764	05	21.077	0.072	20.744	0.030	20.907	0.034	21.046	0.060	21.132	0.216	0.064	000.0	103.4	-50.8						20.775		0.250	DA
000211.15+092909.09	11277-58450-0822	07	21.239	0.079	20.651	0.040	20.434	0.029	20.025	0.035	19.354	0.046	0.098	028.5	103.2	-51.5	3.267	0.778	2.404	0.650	27	20.196	1.175	DA+M	
000211.25+114243.03	11561-58485-0546	12	19.825	0.049	19.436	0.033	19.542	0.022	19.745	0.029	19.909	0.092	0.063	045.1	104.2	-49.4	2.829	0.431	3.179	0.325	36	19.459	-0.007	DA	
000212.38+110905.43	11561-58485-0513	03	22.121	0.161	21.303	0.039	20.877	0.039	20.741	0.052	20.773	0.171	0.057	000.0	104.0	-49.9						20.904		sdA	
000219.56+085915.02	11277-58450-0872	12	21.439	0.096	19.869	0.028	19.116	0.015	18.861	0.018	18.737	0.032	0.058	002.9	103.0	-52.0	0.000	0.436	0.025	0.292	1	19.150	1.027	DZ	
000221.17+090551.44	11277-58450-0830	03	22.153	0.159	21.540	0.053	20.998	0.035	20.943	0.047	20.944	0.177	0.058	000.0	103.1	-51.9						21.064	0.921	sdA	
000329.78+092751.00	11277-58450-0882	05	21.874	0.133	21.064	0.039	20.592	0.033	20.370	0.044	20.588	0.144	0.099	033.4	103.7	-51.6	0.712	0.970	1.583	0.795	3	20.537	0.835	DZ:	
000348.97+100936.80	11561-58485-0419	04	22.807	0.484	20.933	0.039	21.002	0.057	21.028	0.072	21.313	0.406	0.089	000.0	104.1	-51.0						20.885	0.455	DA	
000356.67+110603.64	11561-58485-0612	15	19.651	0.034	19.448	0.025	19.643	0.021	19.886	0.036	20.069	0.107	0.057	034.7	104.6	-50.1	4.739	0.507	5.288	0.366	37	19.519	0.018	DA	
000426.89+104059.93	11561-58485-0396	04	21.611	0.099	21.015	0.036	21.095	0.042	21.071	0.066	20.948	0.194	0.093	000.0	104.6	-50.5						21.041	-0.525	DA	
000444.53+085938.62	11277-58450-0939	06	21.219	0.078	20.670	0.034	20.787	0.033	21.035	0.061	21.233	0.261	0.073	000.0	103.9	-52.1	1.722	1.676	0.707	1.572	25	20.697	0.212	DA	
000457.14+101937.47	09403-58018-0843	13	22.101	0.180	19.564	0.019	18.396	0.014	18.005	0.019	17.765	0.034	0.025	043.9	099.5	-59.6	0.000	0.379	0.297	0.230	42	18.436	0.1507	dC	
000710.54+114549.41	11561-58485-0790	03	23.080	0.476	21.426	0.051	20.852	0.044	20.776	0.056	20.521	0.169	0.084	000.0	106.1	-49.7						20.855	0.357	sdA	
001012.54+105816.47	11561-58485-0099	02	22.246	0.332	21.953	0.138	21.569	0.140	21.443	0.142	21.491	0.352	0.087	000.0	106.9	-50.6	1.997	1.306	1.533	0.951	1	20.594	0.794	DA:	
001140.11+103759.11	11561-58485-0026	08	21.050	0.077	20.288	0.022	19.936	0.022	19.868	0.030	19.745	0.064	0.061	009.0	107.3	-51.0	0.720	0.813	0.236	0.632	2	19.969	0.388	sdA	
001202.04+064945.88	11309-58428-0015	19	20.157	0.040	19.034	0.021	19.070	0.016	19.144	0.020	19.136	0.041	0.057	001.2	105.8	-54.7	0.846	0.645	0.907	0.404	4	18.996	0.329	sdA	
001245.81-010522.66	09402-58039-0891	03	24.122	0.706	21.191	0.040	19.558	0.016	19.069	0.024	18.886	0.037	0.033	050.3	101.7	-62.4	0.826	0.570	0.357	0.417	49	19.650	1.798	dC	

- flux increasing in the red [binary, most probably M companion]
- OI 6 158, 7 774, 8 448Å [DS, oxygen dominated]
- H and He emission lines [CVs and M dwarf companions]

Table 1 is a tally of the 2 410 objects we classified in Table 2. 1404 objects were classified by us as new DAs and only 12 as new DBs. Among the 1 404 DAs, we found 8 magnetic DAs (DAH), 154 showing composite spectra with main-sequence M dwarf companions (DA+M), 46 DAZs with Ca and/or Mg lines, and 6 DABs with H and He I lines. We also found one star with an extremely steep Balmer decrement, i.e. with only a broad H α line while the other lines are absent. It could not be fit with a pure hydrogen grid (see section 2.3 below), or indicated extremely high gravity. We find that this object is best explained as helium-rich DA, and therefore with an extremely thin H layer mixed with the underlying He, and denote it DA(He), as in Kepler et al. (2015, 2016, 2019) (see Fig. 2).

We classified 301 spectra as dC - dwarf carbon stars, in line with Green (2013) and Farihi et al. (2018), but they could also be late type L stars. We do not have spectral models for dCs or L stars, so we do not determine their properties. All 40 CV spectra show both H and He lines, and 11 show also evidence of a disk. Of these CVs, 30 objects already have previous published spectra, and 9 are new cataclysmic variables (see Fig. 3). One new CV has two spectra. We kept the known CVs in the table because their spectra change with time. None shows only He lines, as expected from AM CVns.

We classified 320 stars as sdAs, stars with spectra dominated by narrow hydrogen lines, following Kepler et al. (2016). Solar metallicity main sequence A type stars have absolute magnitudes $M_g \approx 0 - 2$. As stars brighter than $g=14.5$ saturate in SDSS, only main sequence A type stars with distance moduli larger than 12.5 are observed in SDSS, i.e., farther than 3.5 kpc. Because SDSS observed mainly perpendicular to the disk, i.e. galactic latitude in general larger than 30 deg, these would be located in the halo, where most A type dwarf stars should already have evolved off the main sequence. Most of these sdAs stars are likely very low metallicity main sequence stars ($[Fe/H] \lesssim -1.0$), whose spectra are dominated by hydrogen because they lack significant metals (e.g. Chandra & Schlaufman 2021). As their absolute magnitude, according to Gaia parallaxes, cover $M_G \geq 9.5$ they cannot be classified as normal main sequence A type stars. Instead, they likely have masses smaller than the Sun, given their relatively low effective temperatures and location in the *Gaia* colour-magnitude diagram. We also note that they are hotter than sdF stars (Scholz et al. 2015). Some of these sdAs may be stars that lost mass due to binary interaction, resulting most probably in He core stars, precursors of ELMs (Pelisoli, Kepler, & Koester 2018a; Pelisoli et al. 2018b, 2019; Pelisoli & Vos 2019).

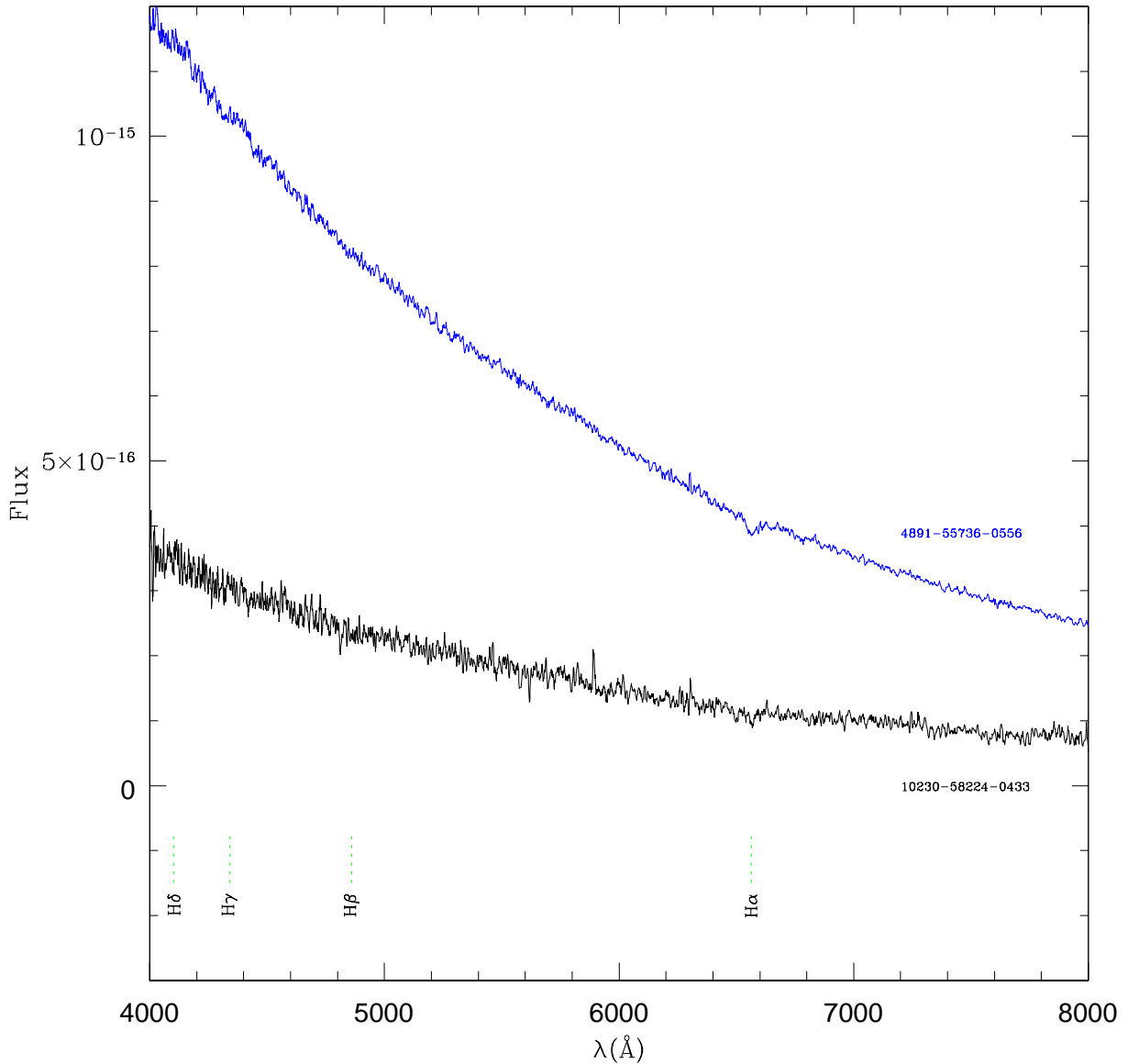


Figure 2. Spectrum of SDSS J095018.83+340743.17, with P-M-F 10230-58224-0433 from DR16 and SDSS J152958.12+130454.80, with P-M-F 4891-55736-0556 from DR14 in blue for comparison, two stars we classified as DA(He) because only a weak H α is detected.

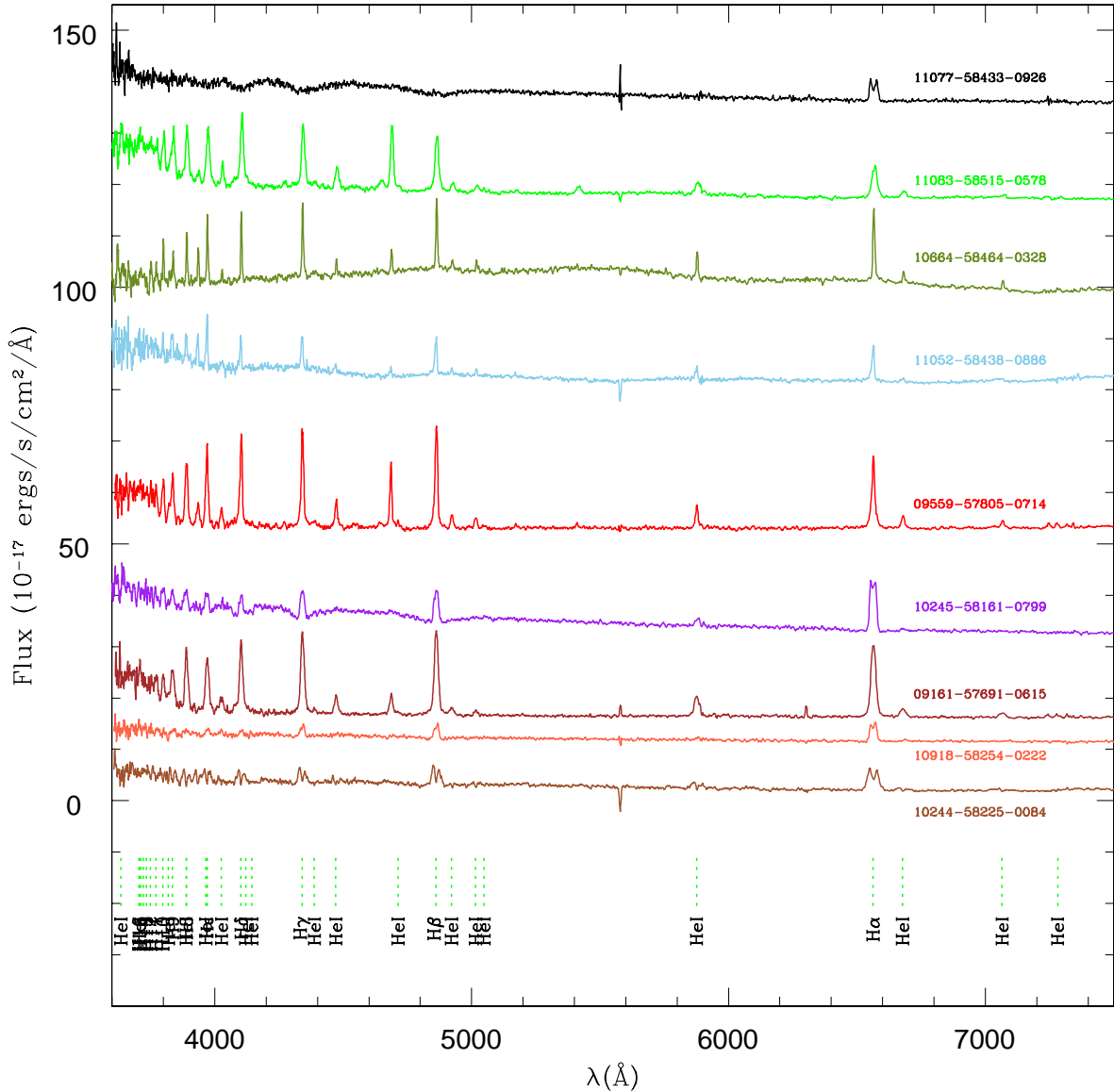


Table 3. Atmospheric parameters for DAs with $(S/N) \geq 10$ and parallax/uncertainty ≥ 4 . The complete table is available in electronic form.

SDSS J	P-M-F	T_{eff}	σ_T	$\log g$	$\sigma_{\log g}$	$V_r (\text{km/s})$	σ_V	S/N	χ^2	d(pc)	z(pc)	E(B-V)	$R_{\star L}$	$M (M_{\odot})$	σ_M
000211.25+114243.06	11561-58485-0546	11832	116	8.125	0.178	+033	02	10.5	0.991	353	268	0.063	0.739	0.674	0.147
000356.67+110603.64	11561-58485-0612	14065	261	8.916	0.105	+167	22	13.7	0.981	211	161	0.057	0.555	1.128	0.070
002015.88+085724.0	11312-58433-0651	08412	061	8.152	0.225	+000	17	08.5	1.065	207	165	0.136	0.563	0.683	0.189
002354.04+072540.33	11313-58426-0562	07940	198	8.463	0.231	+075	47	03.7	0.847	190	155	0.022	0.542	0.880	0.202
004105.49+064152.32	11046-58398-0107	09415	030	8.021	0.063	+000	10	17.1	1.107	168	139	0.024	0.503	0.611	0.049
011526.98+160445.56	11067-58507-0475	12855	205	7.950	0.032	+009	19	12.5	0.994	148	107	0.128	0.415	0.581	0.023
012042.38+151322.53	11067-58507-0210	25278	301	8.145	0.122	+000	16	18.8	1.083	370	271	0.060	0.742	0.708	0.097
012419.71+070726.42	11077-58433-0010	06545	120	7.682	0.374	+012	25	06.1	0.943	215	176	0.032	0.585	0.447	0.223
012458.22+152152.8	11068-58488-0711	31173	273	8.535	0.186	+077	34	12.4	1.215	416	303	0.042	0.780	0.946	0.142
012534.99+160603.50	11059-58515-0473	09755	075	8.644	0.169	+025	26	08.1	1.125	189	136	0.057	0.494	0.993	0.132
012851.81+151311.02	11059-58515-0326	08528	122	7.691	0.029	-015	32	04.0	0.838	123	089	0.032	0.362	0.459	0.016
013436.86+135226.76	11060-58523-0314	26720	322	8.038	0.132	+054	18	16.2	1.017	401	296	0.048	0.773	0.655	0.090
013842.60+082449.66	11071-58429-0748	12267	093	8.085	0.169	+053	12	18.2	1.013	317	252	0.040	0.717	0.652	0.135
014042.04+170048.17	11051-58510-0768	10671	075	8.340	0.195	+006	21	10.3	1.126	257	180	0.057	0.594	0.804	0.172
014102.48+095801.16	11062-58509-0530	08971	077	8.056	0.311	+020	25	06.9	1.004	317	246	0.071	0.709	0.629	0.239
014413.38+140719.39	11052-58438-0354	18275	121	8.003	0.119	+040	12	23.6	0.949	275	200	0.051	0.633	0.620	0.087
014518.98+172343.60	11044-58508-0549	11982	124	8.291	0.168	+013	21	11.1	1.034	316	218	0.043	0.665	0.778	0.147
015436.83+051656.71	11650-58508-0017	11061	455	8.516	0.229	-089	90	02.4	1.122	213	173	0.037	0.580	0.916	0.187
015640.60+142813.13	11045-58485-0858	08708	050	8.122	0.213	+000	15	11.1	1.001	286	204	0.043	0.639	0.666	0.177
072445.68+385044.86	09367-57758-0379	11059	048	7.931	0.097	+084	11	20.3	0.913	223	086	0.055	0.350	0.567	0.067
072559.08+0411245.75	10656-58163-0426	28411	143	8.255	0.138	+012	13	24.9	1.095	366	146	0.063	0.520	0.780	0.112
072559.68+353836.26	09363-57742-0527	18596	107	7.669	0.074	+007	08	30.1	1.104	323	121	0.044	0.454	0.489	0.041
072607.92+035112.08	09367-57758-0733	36766	256	7.998	0.135	-011	16	32.1	0.870	475	188	0.048	0.610	0.654	0.086
072634.39+395440.08	09367-57758-0763	09731	029	8.418	0.062	+067	10	20.0	1.013	146	058	0.047	0.252	0.852	0.056
072655.14+0403027.89	09367-57758-0743	25416	235	7.854	0.225	+043	11	25.4	0.952	505	202	0.043	0.636	0.565	0.126
072902.28+392442.17	09367-57758-0159	11586	081	7.544	0.120	+139	13	16.5	1.056	343	138	0.056	0.498	0.412	0.063
073018.36+111320.42	10656-58163-0276	14194	094	7.792	0.020	+018	08	27.2	1.072	131	054	0.060	0.239	0.522	0.005
073129.34+371444.87	09366-57746-0398	12898	084	8.598	0.034	+057	09	28.2	0.901	114	045	0.048	0.204	0.968	0.029
073237.88+204543.33	10656-58163-0844	17608	044	8.469	0.015	+056	04	63.4	1.087	088	037	0.052	0.172	0.893	0.012
073247.77+213346.81	11085-58462-0525	16899	092	8.117	0.078	-029	10	26.3	1.051	263	083	0.045	0.340	0.679	0.058
073348.71+443733.50	10655-58172-0717	08032	019	7.962	0.044	+099	05	31.3	1.093	118	051	0.054	0.228	0.575	0.034
073357.00+283123.83	10285-58083-0738	16633	186	8.357	0.101	+039	21	13.4	1.086	240	086	0.039	0.352	0.822	0.086
073452.86+380301.56	09366-57746-0762	07592	033	8.085	0.054	+019	07	20.8	1.149	126	052	0.048	0.229	0.642	0.044
073612.36+222937.20	11085-58462-0675	14785	125	8.463	0.027	+079	07	41.8	1.362	136	045	0.039	0.204	0.886	0.023
073619.09+22338.89	11085-58462-0673	23016	131	8.008	0.067	+083	07	36.3	1.074	267	089	0.037	0.362	0.633	0.048
10285-58083-0232	09859	120	7.717	0.104	+160	42	04.9	1.035	260	096	0.036	0.383	0.475	0.063	
103748.13+201835.57	11085-58462-0168	26510	232	8.277	0.141	+084	15	20.5	1.030	382	124	0.036	0.463	0.789	0.117
103812.70+472941.35	10654-58429-0432	24044	110	8.118	0.035	+004	06	42.1	1.159	214	098	0.089	0.389	0.692	0.026

2.3 Theoretical models and fitting methods

The observed spectra for pure DAs, DBs, and DZs were analysed using theoretical LTE (local thermodynamic equilibrium) atmospheric models. The basic principles are described in Koester (2010), but many improvements to the algorithms and models have been included since, as described e.g. in Koester & Kepler (2019); Koester, Kepler, & Irwin (2020). The pure hydrogen DA models use the mixing length approximation for convection with the parameters $\text{MLT2}/\alpha=0.7$; the grid covers the range $5000 \text{ K} \leq T_{\text{eff}} \leq 100\,000 \text{ K}$, $5.0 \leq \log g \leq 9.5 \text{ dex}$ (cgs). The DB grid uses $\text{MLT2}/\alpha = 1.25$, and covers $12\,000 \text{ K} \leq T_{\text{eff}} \leq 45\,000 \text{ K}$, $7.0 \leq \log g \leq 9.5$. This DB grid includes trace hydrogen with logarithmic abundances of $[\text{H}/\text{He}] = -5.0$, which gives a better agreement with the H-rich atmosphere mass distribution (Bergeron et al. 2019; McCleery et al. 2020). The DZ grid uses the 13 most important metals with $Z < 30$, where the metals are in Bulk Earth ratios relative to calcium, and the logarithmic abundance of calcium and helium $[\text{Ca}/\text{He}]$ ranges from -7.0 to -12.0. This ratio is a parameter to be determined along with T_{eff} and $\log g$. The hydrogen abundance was fixed at $[\text{H}/\text{He}] = -4.5$.

Gaia EDR3 (Gaia Collaboration et al. 2021) reported parallaxes for 1473 of our objects, but only 1154 with parallax/error ≥ 1 . A further 181 have parallax in DR2 (Gaia Collaboration et al. 2018), but not EDR3. We used the parallaxes and Gaia G magnitude to estimate the absolute magnitude in the G filter for these objects and used it to distinguish between main sequence stars and subdwarf or white dwarf stars. In our χ^2 fitting procedure, we iterated on the combined observational constraints of the SDSS spectrum, SDSS and Gaia photometry, and Gaia parallaxes. The latter two provide a powerful constraint on the radius and thus $\log g$, and also solve the common degeneracy between hot and cool solutions from the Balmer line fitting. Because of this constraint, we do not apply the 3D corrections of Tremblay et al. (2013) on the result of the spectroscopic fit, since that would imply a change in $\log g$, thus violating the parallax constraint. Statistical errors were derived from the χ^2 fitting; the largest contribution for many objects comes from the parallax error, since we used data with parallax errors up to 25%, corresponding to 0.37 dex in $\log g$.

3 RESULTS

The external uncertainties in our atmospheric parameters derived from spectral analysis are minimized by the use of only SDSS spectra, i.e., same telescope and only one spectrograph (BOSS), and fitting all the spectra with the same models and fitting technique. Table 3 shows the atmospheric parameters we obtained for DAs with $(S/N)_g \geq 10$ and parallax/uncertainty ≥ 4 . The complete table is available as supplementary material. As an example of the fit, Fig 4 shows the measured spectrum and the best fit model for one $(S/N)_g = 70$, $g = 16.639$ mag DA, while Fig. 7 shows the spectrum and a model for one selected DB. All the plots of the fits are made available online.

For 68 DA+dM we fitted the blue part of the spectra to estimate the white dwarf properties, when ignoring the H α line was sufficient for a good fit.

Table 4 shows the parameters for the new 10 DBs with $S/N \geq 10$ following Koester & Kepler (2015).

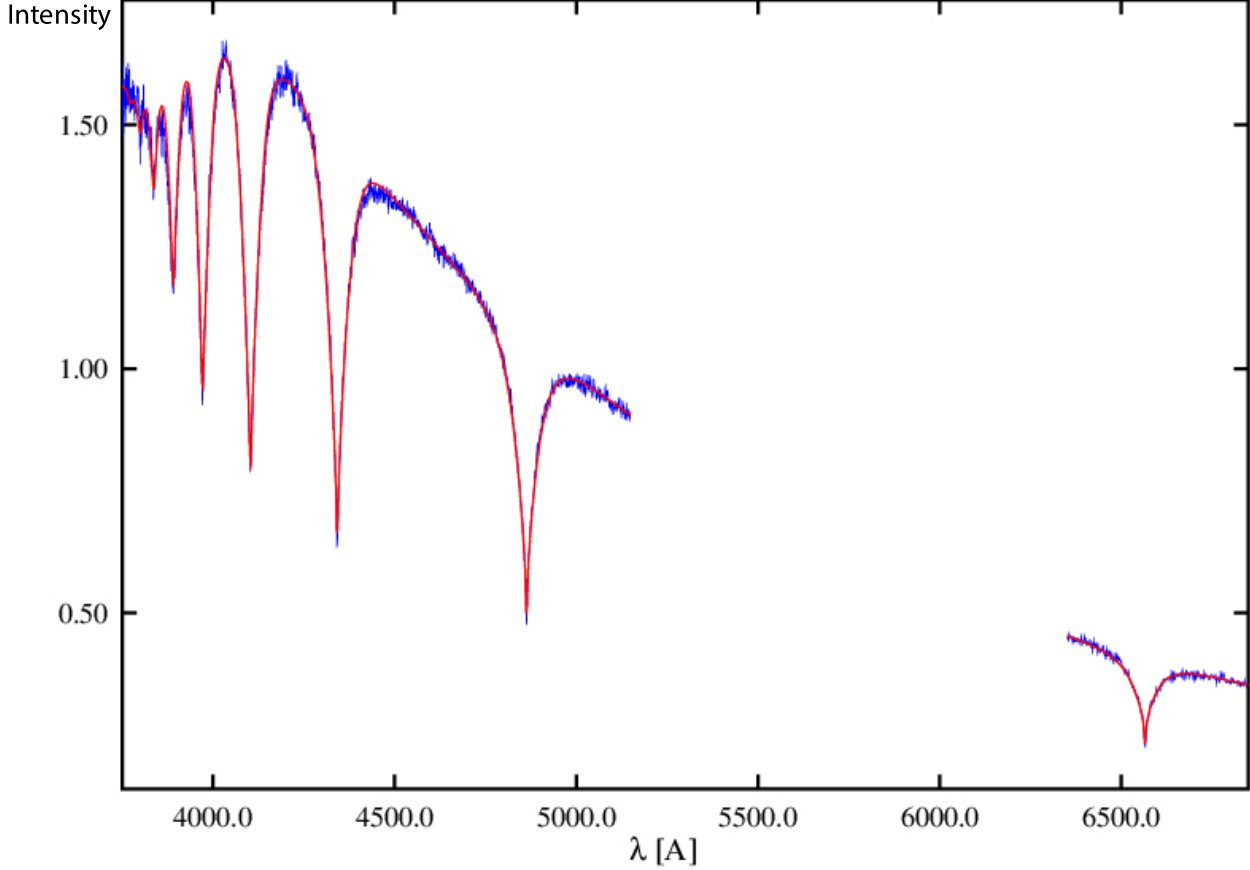


Figure 4. DA SDSS J075144.06+223004.80, $g=16.639$, P-M-F=11112-58428-0632 spectrum in blue, and in red the best model fit at $T_{\text{eff}} = 20056 \pm 46$ K, $\log g = 7.913 \pm 0.025$, mass $M=0.579 \pm 0.017 M_{\odot}$. Only the spectral regions used in our fitting routine are shown. A featureless region for DAs, between H β and H α , is not included in the fit.

Table 4. Atmospheric parameters for DBs

Spectrum	Name	T_{eff}	σ_T	$\log g$	$\sigma_{\log g}$	$V_r(\text{m/s})$	σ_V	S/N	$M(M_{\odot})$	σ_M
09176-58080-0181	SDSSJ2333+0051	19745	170	7.626	0.191	8	7	16.8	0.464	0.034
09355-57814-0682	SDSSJ0804+3513	11573	92	7.990	0.102	38	21	18.7	0.569	0.041
09369-58054-0103	SDSSJ0742+3906	14047	86	7.954	0.184	-8	10	14.9	0.554	0.065
10230-58224-0064	SDSSJ0957+3359	25659	476	8.045	0.075	31	9	18.7	0.629	0.029
10256-58193-0462	SDSSJ1337+3449	18714	118	8.063	0.088	-18	7	19.6	0.626	0.036
10909-58280-0663	SDSSJ1652+3222	16343	46	8.126	0.032	0	5	25.1	0.660	0.014
11123-58429-0222	SDSSJ0839+2553	12643	91	7.972	0.184	-26	12	16.5	0.561	0.067
11350-58455-0130	SDSSJ1010+2722	15258	69	7.630	0.297	0	8	13.4	0.457	0.063
11378-58437-0772	SDSSJ0944+3103	14293	85	7.981	0.239	0	10	13.6	0.570	0.085
11704-58514-0257	SDSSJ0938+2537	16436	60	8.040	0.179	-15	6	19.5	0.609	0.072

3.1 Masses

For white dwarfs, the main indicator of $\log g$ is the width of the atmospheric absorption lines. However, for $T_{\text{eff}} < 10000$ K, the width of the hydrogen lines becomes very weakly dependent on gravity. As a result, it is very difficult to distinguish low mass white dwarfs and metal-poor main sequence A/F stars in the $T_{\text{eff}} < 10000$ K and $\log g < 6.5$ range solely with visual inspection, even though low metallicity main sequence stars have an upper limit to $\log g \lesssim 4.64$, for a turn-off mass of $\sim 0.85 M_{\odot}$. Following Kepler et al. (2019), the two steps we took to overcome this limitation were the extension of our pure H model grid to $\log g \geq 3.5$, fitting all the spectra we visually classified as DAs and sdAs, using the result of the fit to separate $\log g \geq 6.5$ as white dwarfs, and finally, using the parallaxes from Gaia EDR3 to estimate the absolute magnitude and use $M_G \geq 9.5$ as sdAs and white dwarfs, for those spectra showing only hydrogen lines.

At the cool end of our sample, $\log g = 6.5$ corresponds to a mass around $0.2 M_{\odot}$, well below the single mass evolution in the lifetime of

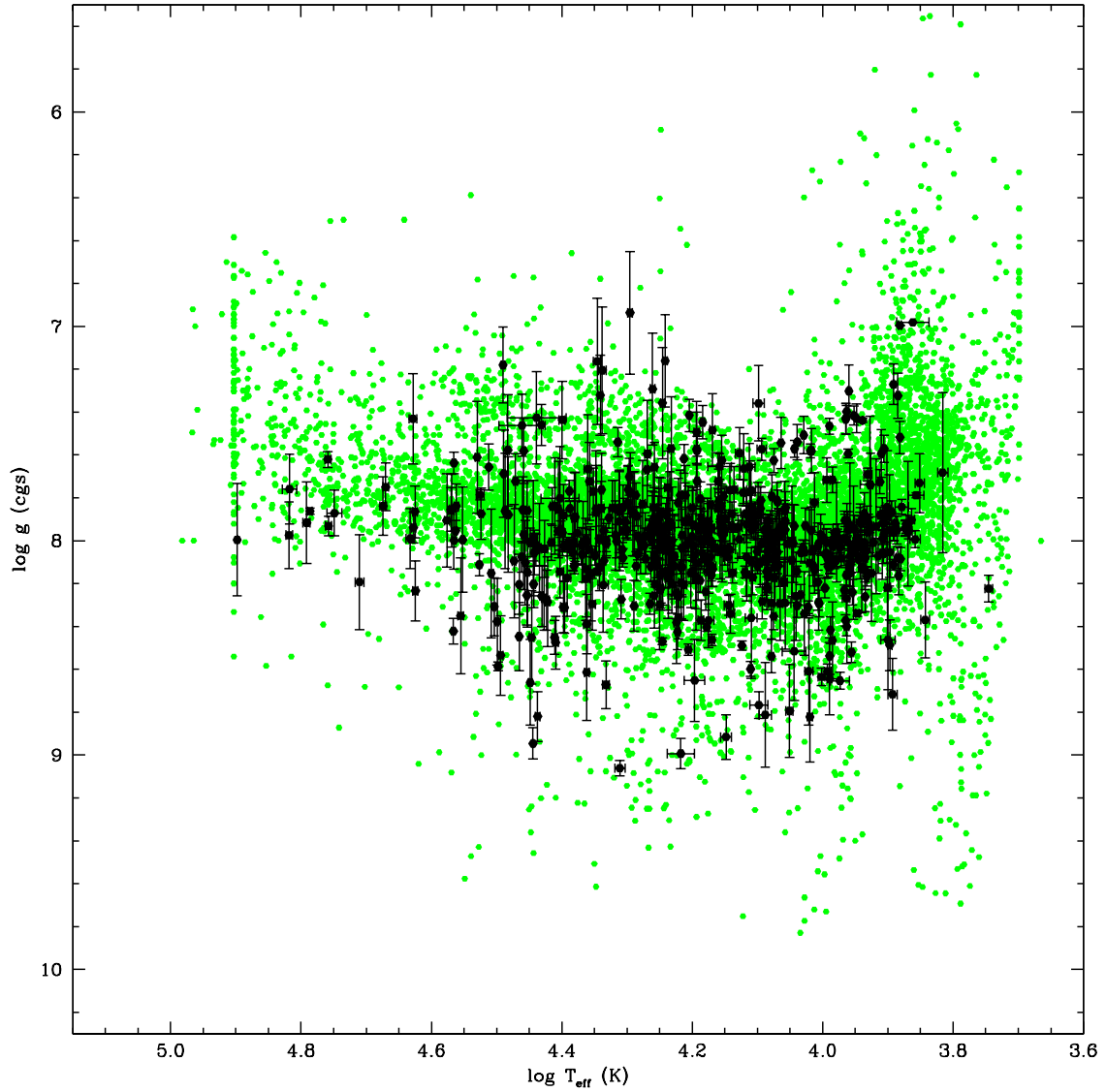


Figure 5. Surface gravity ($\log g$) and effective temperature (T_{eff}) estimated for the 555 pure DA white dwarf stars for which the SDSS spectra has $S/N_g \geq 10$, and Gaia EDR3 parallax/error ≥ 4 . In green, for comparison, the 11 212 pure DAs in [Kepler et al. \(2019\)](#) with $S/N_g \geq 10$.

the Universe — but reachable via interacting binary evolution. The He-core white dwarf stars in the mass range $0.2 - 0.45 M_{\odot}$, referred to as low-mass white dwarfs, are usually found in close binaries, often double degenerate systems (Marsh, Dhillon & Duck 1995), being most likely a product of interacting binary stars evolution. More than 70% of those studied by Kilic et al. (2011) with masses below $0.45 M_{\odot}$ and all but a few with masses below $0.3 M_{\odot}$ show radial velocity variations (Brown et al. 2013; Gianninas et al. 2014; Brown, Kilic, & Gianninas 2017). Kilic, Stanek & Pinsonneault (2007) suggest that single low-mass white dwarfs result from the evolution of old metal-rich stars that truncate evolution before the helium flash due to severe mass loss. They also conclude all white dwarfs with masses below $\simeq 0.3 M_{\odot}$ must be a product of binary star evolution involving interaction between the components.

Table 3 shows the atmospheric parameters obtained from the fitting of the spectra for DAs. The mean mass for these 595 DAs is $\langle M_{\text{DA}} \rangle = 0.6283 \pm 0.0056 M_{\odot}$, where the quoted uncertainty refers to the uncertainty in the mean value itself. The one sigma dispersion of the whole distribution is $0.260 M_{\odot}$. Fig. 8 shows the masses obtained versus effective temperature. A comparison to the masses obtained in Kepler et al. (2019) with the 3D corrections (Tremblay et al. 2013) is also shown in the same figure.

Tremblay et al. (2019) fitted 3171 S/N ≥ 20 SDSS DR14 spectra for DAs white dwarfs selected by Gentile Fusillo et al. (2018), applying 3D corrections and compared to those they obtain from the *Gaia* photometry and parallax, concluding the agreement is good, for DAs, within 2%. They obtained a mean mass $\langle M_{\text{DA}} \rangle = 0.586 M_{\odot}$, with a dispersion of $0.150 M_{\odot}$. For the 1145 DAs in Gianninas, Bergeron, & Ruiz (2011) with good Gaia DR2 parallaxes they obtained a mean mass $\langle M_{\text{DA}} \rangle = 0.599 M_{\odot}$, with a dispersion of $0.165 M_{\odot}$. Genest-Beaulieu & Bergeron (2019) concluded the photometric and spectroscopic analysis of 2236 DAs on their SDSS sample with Gaia DR2 parallaxes/error ≥ 10 agreed within 1σ for 60.9% of their sample and obtained $\langle M_{\text{phot}}^{\text{DA}} \rangle = 0.617 M_{\odot}$, with a dispersion of $0.125 M_{\odot}$ and $\langle M_{\text{spec}}^{\text{DA}} \rangle = 0.615 M_{\odot}$, with a dispersion of $0.147 M_{\odot}$. Kepler et al. (2019) analysed 11 129 DAs up to DR14 with $S/N_g \geq 10$, obtaining a mean mass $\langle M_{\text{DA}} \rangle = 0.5903 \pm 0.0014 M_{\odot}$, and individual dispersion of $0.152 M_{\odot}$. For the 8171 DAs with $T_{\text{eff}} \geq 10\,000$ K, the mean mass was $\langle M_{\text{DA}} \rangle = 0.6131 \pm 0.0014 M_{\odot}$, with a dispersion $0.126 M_{\odot}$, while for those 2958 with $T_{\text{eff}} < 10\,000$ K, $\langle M_{\text{DA}} \rangle = 0.5276 \pm 0.0035 M_{\odot}$ with a dispersion $0.174 M_{\odot}$. The DR16 sample is not large enough to allow a study of the mass distribution and its dependency with temperature. A future work analysing the whole SDSS sample with a consistent method and parallax will be necessary.

With Gaia DR2 and EDR3 parallaxes, we were also able to fit simultaneously the photometry and spectra for 85 SDSS DZs with $S/N_g \geq 20$ and parallax/error ≥ 4 , estimating their effective temperatures, surface gravities and [Ca/H] (see Fig. 10). These objects were not restricted to DR16. In fact, only 3 DZs in DR16 have $S/N_g \geq 20$, P-M-F=09161-57691-0879 SDSS J212140.24+021737.32, 09174-58070-0242 SDSS J231317.47+001201.16 and 10910-58254-0644 SDSS J162625.86+351341.48, but none with parallax/error ≥ 4 . Fig. 9 shows one sample DZ spectra and our best fit model.

For DZs, we estimated their T_{eff} and $\log g$ from new atmospheric models. The mean parameters for the 85 analysed DZs range from 13870 K to 5900 K and 7.762 to 8.329 dex are $\langle T_{\text{eff}}^{\text{DZ}} \rangle = 8685 \pm 1586$ K and $\langle \log g_{\text{DZ}} \rangle = 8.017 \pm 0.011$ dex(cgs) (weighted mean 8.020 dex), and a mean mass of $\langle M_{\text{DZ}} \rangle = 0.640 \pm 0.013 M_{\odot}$, compared to the sample of 555 DAs, ranging from $79\,000 \leq T_{\text{eff}} \leq 5\,600$ K, $6.937 \leq \log g \leq 9.061$ dex $\langle T_{\text{eff}}^{\text{DA}} \rangle = 16803 \pm 380$ K, $\langle \log g_{\text{DA}} \rangle = 7.998 \pm 0.011$, and mean mass $\langle M_{\text{DA}} \rangle = 0.618 \pm 0.006 M_{\odot}$, and a one sigma dispersion of $0.123 M_{\odot}$. Fig. 11 shows the calcium determinations for the sample. The sample reported is not large enough to allow a study of the mass distribution for a meaningful comparison with the DA or DB mean mass, and the dependency of the calcium abundances with temperature due to the deepening of the convection zone at lower temperatures.

4 CONCLUSIONS

We extended our search for new spectroscopically confirmed white dwarf and subdwarf stars to SDSS DR16. The SDSS flux calibration is based on hundreds of comparison stars and in general more accurate than those derived from single night observations. We fit the spectra of the highest signal-to-noise for each star, taking into account that SDSS re-observes fields and improves the quality of the spectra.

The total number of unique stars in Kleinman et al. (2013); Kepler et al. (2015, 2016, 2019) and this paper is 30 086 DAs, 2390 DCs, 2160 DBs, 1316 DZs, 572 DQs, 137 DOs, 4 DS, 396 sdB, 410 sdOs, and 363 CVs, i.e., DAs correspond to 82% of the white dwarfs with SDSS spectra, excluding subdwarfs and CVs.

After the conclusion of our work, Gentile Fusillo et al. (2021) submitted a visual classification of 998 DR16 spectra, 777 in common with our sample, and our classifications agree. Their remaining 221 spectra are either re-observations of already classified white dwarfs or not white dwarfs.

5 DATA AVAILABILITY

The data underlying this article are available in the article and in its online supplementary material. The spectra are available on the Sloan Digital Sky Survey databases.

Table 5. Parameters for the 85 DZs with $(S/N)_g \geq 20$ SDSS spectra and Gaia EDR3 parallaxes, for models with metals fixed at bulk Earth (B.E.) ratios to Ca, [Ca/He] from -7.00 to -15.00.

P-M-F	Name	T_{eff}	σ_T	$\log g$	$\sigma_{\log g}$	$m\text{-M}$	$\sigma_{m\text{-}M}$	d[pc]	z[pc]	E(B-V)	R_A	-[Ca/He]	$\sigma_{[\text{Ca}/\text{He}]}$	V_r	σ_V	S/N	M	σ_M
0305-51613-0197	SDSSJ1425-0050	07131	068	8.191	0.052	4.249	0.031	0070	0057	0.042	0.249	10.799	0.031	012	33	14.1	0.887	0.111
0335-52000-0247	SDSSJ1234-0330	08809	142	8.065	0.050	5.148	0.053	0107	0091	0.031	0.368	10.554	0.040	026	17	16.0	0.608	0.021
0447-51877-0499	SDSSJ0848+5214	08130	077	8.011	0.041	5.128	0.050	0106	0066	0.021	0.283	10.535	0.029	094	15	15.1	0.573	0.018
0655-52162-0300	SDSSJ0036-1112	07192	050	8.097	0.019	3.594	0.012	0052	0050	0.026	0.222	09.284	0.017	159	13	16.1	0.625	0.129
0660-52177-0277	SDSSJ0113-0959	10455	189	7.943	0.045	5.568	0.038	0129	0123	0.031	0.461	08.567	0.025	044	06	16.5	0.539	0.017
0737-52518-0009	SDSSJ2228+1207	06696	032	8.019	0.014	2.653	0.006	0033	0020	0.074	0.098	09.753	0.007	116	06	23.7	0.879	0.001
0934-52627-0553	SDSSJ0848+5348	07832	089	8.180	0.040	4.753	0.045	0089	0055	0.027	0.242	10.318	0.017	041	14	16.1	0.678	0.018
1010-52649-0084	SDSSJ1049+5154	06532	060	7.811	0.034	4.504	0.028	0079	0066	0.008	0.282	09.930	0.021	130	19	10.1	0.872	0.001
1281-52753-0439	SDSSJ1309+4913	08284	078	7.996	0.022	4.484	0.015	0078	0072	0.006	0.305	09.972	0.013	048	07	19.3	0.564	0.009
1319-52791-0409	SDSSJ1313+5738	08694	090	7.987	0.022	4.162	0.008	0067	0058	0.010	0.253	09.194	0.010	000	04	26.2	0.559	0.009
1345-52814-0032	SDSSJ1351+4253	06424	051	8.088	0.022	2.977	0.006	0039	0037	0.008	0.169	11.212	0.031	089	44	18.6	0.882	0.001
1655-53523-0127	SDSSJ1558+2512	07196	065	8.058	0.023	3.663	0.010	0054	0040	0.056	0.183	10.753	0.018	129	17	20.4	0.601	0.140
1691-53260-0265	SDSSJ1647+2636	06984	060	7.986	0.022	3.518	0.007	0050	0030	0.074	0.143	09.830	0.010	090	09	18.4	0.878	0.001
1694-53472-0154	SDSSJ1246+1155	07995	088	8.016	0.029	4.513	0.023	0079	0077	0.023	0.320	08.301	0.058	090	16	13.6	0.576	0.012
2037-53446-0579	SDSSJ1125+3823	10154	171	8.056	0.053	5.590	0.063	0131	0122	0.016	0.458	08.618	0.021	094	07	17.0	0.605	0.022
2170-53875-0154	SDSSJ1554+1735	05900	029	7.762	0.021	3.753	0.016	0056	0041	0.030	0.186	10.196	0.022	166	27	09.3	0.871	0.001
2301-53712-0599	SDSSJ0618+6413	08753	142	7.925	0.088	6.353	0.106	0186	0066	0.090	0.282	10.264	0.024	025	11	15.4	0.524	0.030
2367-53763-0546	SDSSJ1034+2245	06676	032	8.012	0.015	3.053	0.009	0040	0034	0.017	0.160	09.317	0.012	130	08	22.9	0.879	0.001
2406-54084-0328	SDSSJ1005+2655	07859	104	7.965	0.084	5.756	0.105	0141	0113	0.025	0.432	09.726	0.015	088	10	16.2	0.545	0.032
2421-54153-0336	SDSSJ0809+1112	06356	046	8.092	0.022	3.602	0.016	0052	0020	0.029	0.095	11.312	0.044	048	77	12.5	0.882	0.001
2512-53877-0570	SDSSJ1156+1822	07154	044	8.015	0.017	2.133	0.004	0026	0025	0.027	0.121	11.748	0.052	092	46	42.3	0.580	0.149
2629-54087-0330	SDSSJ2305+2307	11853	239	8.051	0.078	6.477	0.104	0197	0109	0.171	0.421	08.160	0.024	-06	04	25.9	0.606	0.033
2907-54580-0126	SDSSJ1428+4403	06221	033	7.886	0.018	3.261	0.006	0044	0040	0.011	0.183	09.756	0.022	095	22	10.8	0.874	0.001
2922-54612-0509	SDSSJ1244+0118	08203	104	8.060	0.093	6.126	0.124	0167	0147	0.029	0.522	08.002	0.001	-46	01	09.6	0.603	0.041
3236-54892-0599	SDSSJ1258+3047	07233	088	8.072	0.072	5.343	0.094	0117	0116	0.010	0.442	10.971	0.027	095	36	14.8	0.610	0.139
3251-54882-0406	SDSSJ1046+2424	06160	045	8.033	0.027	3.858	0.024	0059	0052	0.030	0.229	11.162	0.025	075	38	18.5	0.879	0.001
3428-54979-0618	SDSSJ1616+4600	06100	050	8.006	0.030	4.613	0.026	0083	0059	0.010	0.258	10.449	0.020	083	24	11.3	0.878	0.001
3480-54999-0359	SDSSJ1640+3154	06743	057	8.015	0.041	5.239	0.050	0111	0072	0.021	0.304	09.899	0.019	117	19	10.4	0.879	0.001
3609-55201-0385	SDSSJ2020-0039	09373	123	7.977	0.039	5.229	0.039	0111	0094	0.024	0.378	08.459	0.013	053	04	25.9	0.555	0.016
3752-55236-0550	SDSSJ0749+3124	06572	059	8.084	0.043	4.806	0.051	0091	0039	0.050	0.178	09.988	0.012	092	10	15.3	0.882	0.001
3775-55207-0079	SDSSJ1143-0145	09046	172	7.840	0.148	6.581	0.189	0207	0173	0.014	0.580	09.933	0.017	097	06	19.1	0.494	0.038
3814-55535-0008	SDSSJ09000+0331	07810	085	8.020	0.051	5.326	0.064	0116	0058	0.052	0.253	11.167	0.058	104	38	16.7	0.578	0.022
3818-55532-0016	SDSSJ0909-0045	08674	142	8.004	0.114	6.475	0.158	0197	0098	0.027	0.388	09.346	0.016	115	08	16.6	0.570	0.046
3835-55570-0386	SDSSJ1049-0007	09092	107	7.891	0.132	6.512	0.165	0200	0153	0.036	0.536	08.255	0.027	059	11	14.3	0.510	0.040
3840-55574-0125	SDSSJ1137-0023	09484	215	8.063	0.147	6.650	0.204	0213	0179	0.017	0.593	09.798	0.021	000	07	17.1	0.608	0.062
3861-55274-0690	SDSSJ1353+3239	08039	098	7.924	0.042	5.263	0.037	0112	0109	0.011	0.421	10.732	0.014	034	09	28.8	0.522	0.014
3955-55678-0456	SDSSJ1516+2118	09183	103	8.096	0.034	5.158	0.036	0107	0089	0.045	0.362	10.579	0.027	026	10	27.5	0.627	0.015
4007-55327-0548	SDSSJ1037+0307	08159	098	7.949	0.064	5.646	0.075	0134	0122	0.023	0.459	09.842	0.019	051	11	12.7	0.536	0.024
4035-55383-0874	SDSSJ1414-0113	08525	111	7.878	0.042	5.175	0.038	0108	0089	0.046	0.359	10.594	0.013	025	05	35.9	0.505	0.010
4065-55638-0194	SDSSJ1633+4122	06420	053	8.043	0.031	4.395	0.031	0075	0043	0.060	0.194	11.352	0.028	262	48	20.1	0.880	0.001
4180-56079-0030	SDSSJ1703+2541	08904	105	7.969	0.033	5.199	0.028	0109	0061	0.031	0.265	10.265	0.013	029	06	26.7	0.549	0.013
4218-55479-0010	SDSSJ0048-0112	09390	138	7.994	0.061	5.900	0.076	0151	0133	0.023	0.487	09.592	0.013	041	04	25.9	0.565	0.025
4226-55475-0310	SDSSJ106-0103	11545	266	7.939	0.132	6.778	0.171	0226	0203	0.054	0.638	08.233	0.026	-01	04	20.3	0.539	0.046
4238-55455-0226	SDSSJ0229-0041	08140	119	8.084	0.084	5.954	0.113	0155	0126	0.029	0.469	10.895	0.029	023	26	17.0	0.618	0.037
4395-55828-0220	SDSSJ0218-0919	09733	123	8.037	0.031	4.915	0.025	0096	0085	0.023	0.348	10.106	0.016	085	05	30.1	0.592	0.013
4483-55587-0348	SDSSJ0823+2015	10302	247	7.939	0.116	6.716	0.142	0220	0106	0.034	0.414	09.116	0.020	049	04	20.8	0.536	0.040
4489-55545-0877	SDSSJ0838+3146	08175	105	7.852	0.089	5.828	0.108	0146	0074	0.027	0.313	11.103	0.042	066	20	20.3	0.496	0.021
4543-55888-0238	SDSSJ0046+0704	09024	151	8.006	0.070	5.762	0.088	0142	0117	0.038	0.444	09.714	0.010	036	04	29.3	0.572	0.029
4567-55889-0828	SDSSJ1052+2418	07308	056	8.031	0.022	3.616	0.014	0052	0031	0.112	0.146	09.389	0.007	161	04	33.5	0.584	0.010
5120-56003-0448	SDSSJ1547+0659	08367	079	7.931	0.027	4.716	0.022	0087	0060	0.029	0.261	09.616	0.008	083	04	27.5	0.526	0.010
5314-55952-0385	SDSSJ0934+0822	08939	096	8.028	0.049	5.219	0.063	0110	0070	0.034	0.299	09.665	0.011	096	04	25.5	0.585	0.021
5344-55924-0684	SDSSJ1031+0936	10672	258	7.996	0.113	6.516	0.151	0200	0159	0.030	0.550	10.208	0.043	040	13	17.5	0.570	0.045
5472-55976-0148	SDSSJ1441+0831	07083	077	8.006	0.060	5.019	0.078	0100	0085	0.025	0.348	10.730	0.017	104	16	19.3</td		

de Astrofísica de Canarias, The Johns Hopkins University, Kavli Institute for the Physics and Mathematics of the Universe (IPMU) / University of Tokyo, Lawrence Berkeley National Laboratory, Leibniz Institut für Astrophysik Potsdam (AIP), Max-Planck-Institut für Astronomie (MPIA Heidelberg), Max-Planck-Institut für Astrophysik (MPA Garching), Max-Planck-Institut für Extraterrestrische Physik (MPE), National Astronomical Observatories of China, New Mexico State University, New York University, University of Notre Dame, Observatório Nacional / MCTI, The Ohio State University, Pennsylvania State University, Shanghai Astronomical Observatory, United Kingdom Participation Group, Universidad Nacional Autónoma de México, University of Arizona, University of Colorado Boulder, University of Oxford, University of Portsmouth, University of Utah, University of Virginia, University of Washington, University of Wisconsin, Vanderbilt University, and Yale University.

This research has made use of NASA's Astrophysics Data System Bibliographic Services, SIMBAD database, operated at CDS, Strasbourg, France, and IRAF, distributed by the National Optical Astronomy Observatory, which is operated by the Association of Universities for Research in Astronomy (AURA) under a cooperative agreement with the National Science Foundation. This work presents results from the European Space Agency (ESA) space mission Gaia. Gaia data are being processed by the Gaia Data Processing and Analysis Consortium (DPAC). Funding for the DPAC is provided by national institutions, in particular the institutions participating in the Gaia MultiLateral Agreement (MLA). The Gaia mission website is <https://www.cosmos.esa.int/gaia>. The Gaia archive website is <https://archives.esac.esa.int/gaia>.

The Gaia mission and data processing have financially been supported by, in alphabetical order by country: the Algerian Centre de Recherche en Astronomie, Astrophysique et Géophysique of Bouzareah Observatory; the Austrian Fonds zur Förderung der wissenschaftlichen Forschung (FWF) Hertha Firberg Programme through grants T359, P20046, and P23737; the BELgian federal Science Policy Office (BELSPO) through various PROgramme de D'veloppement d'Expériences scientifiques (PRODEX) grants and the Polish Academy of Sciences - Fonds Wetenschappelijk Onderzoek through grant VS.091.16N; the Brazil-France exchange programmes Fundação de Amparo à Pesquisa do Estado de São Paulo (FAPESP) and Coordenação de Aperfeiçoamento de Pessoal de Nível Superior (CAPES) - Comité Français d'Evaluation de la Coopération Universitaire et Scientifique avec le Brésil (COFECUB); the Chilean Dirección de Gestión de la Investigación (DGI) at the University of Antofagasta and the Comité Mixto ESO-Chile; the National Science Foundation of China (NSFC) through grants 11573054 and 11703065; the Czech-Republic Ministry of Education, Youth, and Sports through grant LG 15010, the Czech Space Office through ESA PECS contract 98058, and Charles University Prague through grant PRIMUS/SCI/17; the Danish Ministry of Science; the Estonian Ministry of Education and Research through grant IUT40-1; the European Commission's Sixth Framework Programme through the European Leadership in Space Astrometry (ELSA) Marie Curie Research Training Network (MRTN-CT-2006-033481), through Marie Curie project PIOF-GA-2009-255267 (Space AsteroSeismology & RR Lyrae stars, SAS-RRL), and through a Marie Curie Transfer-of-Knowledge (ToK) fellowship (MTKD-CT-2004-014188); the European Commission's Seventh Framework Programme through grant FP7-606740 (FP7-SPACE-2013-1) for the Gaia European Network for Improved data User Services (GENIUS) and through grant 264895 for the Gaia Research for European Astronomy Training (GREAT-ITN) network; the European Research Council (ERC) through grants 320360 and 647208 and through the European Union's Horizon 2020 research and innovation programme through grants 670519 (Mixing and Angular Momentum tranSport of massIvE stars - MAMSIE) and 687378 (Small Bodies: Near and Far); the European Science Foundation (ESF), in the framework of the Gaia Research for European Astronomy Training Research Network Programme (GREAT-ESF); the European Space Agency (ESA) in the framework of the Gaia project, through the Plan for European Cooperating States (PECS) programme through grants for Slovenia, through contracts C98090 and 4000106398/12/NL/KML for Hungary, and through contract 4000115263/15/NL/IB for Germany; the European Union (EU) through a European Regional Development Fund (ERDF) for Galicia, Spain; the Academy of Finland and the Magnus Ehrnrooth Foundation; the French Centre National de la Recherche Scientifique (CNRS) through action 'Défi MASTODONS' the Centre National d'Etudes Spatiales (CNES), the L'Agence Nationale de la Recherche (ANR) 'Investissements d'avenir' Initiatives D'EXcellence (IDEX) programme Paris Sciences et Lettres (PSL**) through grant ANR-10-IDEX-0001-02, the ANR D'efi de tous les savoirs' (DS10) programme through grant ANR-15-CE31-0007 for project 'Modelling the Milky Way in the Gaia era' (MOD4Gaia), the Région Aquitaine, the Université de Bordeaux, and the Utinam Institute of the Université de Franche-Comté, supported by the Région de Franche-Comté and the Institut des Sciences de l'Univers (INSU); the German Aerospace Agency (Deutsches Zentrum für Luft- und Raumfahrt e.V., DLR) through grants 50QG0501, 50QG0601, 50QG0602, 50QG0701, 50QG0901, 50QG1001, 50QG1101, 50QG1401, 50QG1402, 50QG1403, and 50QG1404 and the Centre for Information Services and High Performance Computing (ZIH) at the Technische Universität (TU) Dresden for generous allocations of computer time; the Hungarian Academy of Sciences through the Lendület Programme LP2014-17 and the János Bolyai Research Scholarship (L. Molnár and E. Plachy) and the Hungarian National Research, Development, and Innovation Office through grants NKFIH K-115709, PD-116175, and PD-121203; the Science Foundation Ireland (SFI) through a Royal Society - SFI University Research Fellowship (M. Fraser); the Israel Science Foundation (ISF) through grant 848/16; the Agenzia Spaziale Italiana (ASI) through contracts I/037/08/0, I/058/10/0, 2014-025-R.0, and 2014-025-R.1.2015 to the Italian Istituto Nazionale di Astrofisica (INAF), contract 2014-049-R.0/1/2 to INAF dedicated to the Space Science Data Centre (SSDC, formerly known as the ASI Science Data Centre, ASDC), and contracts I/008/10/0, 2013/030/I.0, 2013-030-I.0.1-2015, and 2016-17-I.0 to the Aerospace Logistics Technology Engineering Company (ALTEC S.p.A.), and INAF; the Netherlands Organisation for Scientific Research (NWO) through grant NWO-M-614.061.414 and through a VICI grant (A. Helmi) and the Netherlands Research School for Astronomy (NOVA); the Polish National Science Centre through HARMONIA grant 2015/18/M/ST9/00544 and ETIUDA grants 2016/20/S/ST9/00162 and 2016/20/T/ST9/00170; the Portuguese Fundação para a Ciência e a Tecnologia (FCT) through grant SFRH/BPD/74697/2010; the Strategic Programmes UID/FIS/00099/2013 for CENTRA and UID/EEA/00066/2013 for UNINOVA; the Slovenian Research Agency through grant P1-0188; the Spanish Ministry of Economy (MINECO/FEDER, UE) through grants ESP2014-55996-C2-1-R, ESP2014-55996-C2-2-R, ESP2016-80079-C2-1-R, and ESP2016-80079-C2-2-R, the Spanish Ministerio de Economía, Industria y

Competitividad through grant AyA2014-55216, the Spanish Ministerio de Educación, Cultura y Deporte (MECD) through grant FPU16/03827, the Institute of Cosmos Sciences University of Barcelona (ICCUB, Unidad de Excelencia 'María de Maeztu') through grant MDM-2014-0369, the Xunta de Galicia and the Centros Singulares de Investigación de Galicia for the period 2016-2019 through the Centro de Investigación en Tecnologías de la Información y las Comunicaciones (CITIC), the Red Española de Supercomputación (RES) computer resources at MareNostrum, and the Barcelona Supercomputing Centre - Centro Nacional de Supercomputación (BSC-CNS) through activities AECT-2016-1-0006, AECT-2016-2-0013, AECT-2016-3-0011, and AECT-2017-1-0020; the Swedish National Space Board (SNSB/Rymdstyrelsen); the Swiss State Secretariat for Education, Research, and Innovation through the ESA PRODEX programme, the Mesures d'Accompagnement, the Swiss Activités Nationales Complémentaires, and the Swiss National Science Foundation; the United Kingdom Rutherford Appleton Laboratory, the United Kingdom Science and Technology Facilities Council (STFC) through grant ST/L006553/1, the United Kingdom Space Agency (UKSA) through grant ST/N000641/1 and ST/N001117/1, as well as a Particle Physics and Astronomy Research Council Grant PP/C503703/1.

REFERENCES

- Ahumada R., Allende Prieto C., Almeida A., Anders F., Anderson S. F., Andrews B. H., Anguiano B., et al., 2020, *ApJS*, 249, 3. doi:10.3847/1538-4365/ab929e
 Allende Prieto C., et al., 2008, *AJ*, 136, 2070
 Barstow M. A., Barstow J. K., Casewell S. L., Holberg J. B., Hubeny I., 2014, *MNRAS*, 440, 1607
 Bergeron P., Saffer R. A., Liebert J., 1992, *ApJ*, 394, 228
 Bergeron P., Dufour P., Fontaine G., Couto S., Blouin S., Genest-Beaulieu C., Bédard A., et al., 2019, *ApJ*, 876, 67. doi:10.3847/1538-4357/ab153a
 Blouin S., Dufour P., 2019, *MNRAS*, 490, 4166. doi:10.1093/mnras/stz2915
 Brown W. R., Kilic M., Allende Prieto C., Gianninas A., Kenyon S. J., 2013, *ApJ*, 769, 66
 Brown W. R., Kilic M., Gianninas A., 2017, *ApJ*, 839, 23
 Bruhweiler F. C., Kondo Y., 1983, *ApJ*, 269, 657. doi:10.1086/161073
 Calcaferro L. M., Althaus L. G., Cársico A. H., 2018, *A&A*, 614, A49
 Chandra V., Schlaufman K. C., 2021, *AJ*, 161, 197. doi:10.3847/1538-3881/abe535
 Chandrasekhar S., 1931, *ApJ*, 74, 81. doi:10.1086/143324
 Chandrasekhar S., Tooper R. F., 1964, *ApJ*, 139, 1396. doi:10.1086/147883
 Cársico A. H., Romero A. D., Althaus L. G., Hermes J. J., 2012, *A&A*, 547, A96
 Chayer P., Bergeron P., Fontaine G., Wesemael F., 1989, *JRASC*, 83, 325
 Doherty C. L., Gil-Pons P., Siess L., Lattanzio J. C., Lau H. H. B., 2015, *MNRAS*, 446, 2599.
 Eisenstein, D. J., et al. 2006, *ApJS*, 167, 40
 El-Badry K., Rix H.-W., 2018, *MNRAS*, 480, 4884
 Farihi J., Arendt A. R., Machado H. S., Whitehouse L. J., 2018, *MNRAS*, 477, 3801
 Gaia Collaboration, Brown A. G. A., Vallenari A., Prusti T., de Bruijne J. H. J., Babusiaux C., Bailer-Jones C. A. L., et al., 2018, *A&A*, 616, A1. doi:10.1051/0004-6361/201833051
 Gaia Collaboration, Brown A. G. A., Vallenari A., Prusti T., de Bruijne J. H. J., Babusiaux C., Biermann M., et al., 2021, *A&A*, 650, C3. doi:10.1051/0004-6361/202039657e
 Genest-Beaulieu C., Bergeron P., 2019, *ApJ*, 871, 169. doi:10.3847/1538-4357/aafac6
 Gentile Fusillo N. P., et al., 2018, *MNRAS*, 482, 4570
 Gentile Fusillo N. P., Tremblay P.-E., Cukanovaite E., Vorontseva A., Lallement R., Hollands M., Gänsicke B. T., et al., 2021, arXiv, arXiv:2106.07669
 Gianninas A., Bergeron P., Ruiz M. T., 2011, *ApJ*, 743, 138. doi:10.1088/0004-637X/743/2/138
 Gianninas A., Dufour P., Kilic M., Brown W. R., Bergeron P., Hermes J. J., 2014, *ApJ*, 794, 35
 Green P., 2013, *ApJ*, 765, 12
 Heber, U., Reid, I. N., & Werner, K. 2000, *A&A*, 363, 198
 Heber U., 2016, *PASP*, 128, 082001
 Hollands M. A., Gänsicke B. T., Koester D., 2018, *MNRAS*, 477, 93. doi:10.1093/mnras/sty592
 Hollands M. A., Koester D., Alekseev V., Herbert E. L., Gänsicke B. T., 2017, *MNRAS*, 467, 4970. doi:10.1093/mnras/stx250
 Ibeling D., Heger A., 2013, *ApJ*, 765, L43
 Istrate A. G., Marchant P., Tauris T. M., Langer N., Stancliffe R. J., Grassitelli L., 2016, *A&A*, 595, A35
 Kepler S. O., et al., 2015, *MNRAS*, 446, 4078
 Kepler S. O., et al., 2016, *MNRAS*, 455, 3413
 Kepler S. O., Pelisoli I., Koester D., Reindl N., Geier S., Romero A. D., Ourique G., et al., 2019, *MNRAS*, 486, 2169. doi:10.1093/mnras/stz960
 Kilic M., Stanek K. Z., Pinsonneault M. H., 2007, *ApJ*, 671, 761
 Kilic M., Brown W. R., Allende Prieto C., Agüeros M. A., Heinke C., Kenyon S. J., 2011, *ApJ*, 727, 3
 Kilic M., Bergeron P., Blouin S., Bédard A., 2021, *MNRAS.tmp*. doi:10.1093/mnras/stab767
 Kleinman S. J., Kepler S.O., Koester D., Pelisoli I., Peçanha V., Nitta A., Costa J.E.S., Krzesiński J., et al. 2013, *ApJS*, 204, 5.
 Koester D., Kepler, S.O., 2015, *A&A*, 583, A86. doi:10.1051/0004-6361/201527169
 Koester D., Schulz H., Weidemann V., 1979, *A&A*, 76, 262
 Koester D., Weidemann V., Zeidler E.-M., 1982, *A&A*, 116, 147
 Koester D., 2010, *Mem. Soc. Astron. Ital.*, 81, 921
 Koester D., Gänsicke B. T., Farihi J., 2014, *A&A*, 566, A34
 Koester D., Kepler S. O., 2019, *A&A*, 628, A102. doi:10.1051/0004-6361/201935946
 Koester D., Kepler S. O., Irwin A. W., 2020, *A&A*, 635, A103. doi:10.1051/0004-6361/202037530
 Lauffer, G. R., Romero, A. D., & Kepler, S. O. 2018, *MNRAS*, 480, 1547
 Lee Y. S., et al., 2008, *AJ*, 136, 2050

- Lee Y. S., et al., 2008, AJ, 136, 2022
- Li Z., Chen X., Chen H.-L., Han Z. 2019, ApJ, 871, 148
- Margala D., Kirkby D., Dawson K., Bailey S., Blanton M., Schneider D. P., 2016, ApJ, 831, 157
- Marsh T. R., Dhillon V. S., Duck S. R., 1995, MNRAS, 275, 828
- Maxted P. F. L., et al., 2014a, MNRAS, 437, 1681
- Maxted P. F. L., Serenelli A. M., Marsh T. R., Catalán S., Mahtani D. P., Dhillon V. S., 2014b, MNRAS, 444, 208
- McCleery J., Tremblay P.-E., Gentile Fusillo N. P., Hollands M. A., Gänsicke B. T., Izquierdo P., Toonen S., et al., 2020, MNRAS, 499, 1890. doi:10.1093/mnras/staa2030
- Michaud G., Alecian G., Richer J., 2015, ads..book. doi:10.1007/978-3-319-19854-5
- Pelisoli I., Kepler S. O., Koester D., 2018, MNRAS, 475, 2480
- Pelisoli I., Kepler S. O., Koester D., Castanheira B. G., Romero A. D., Fraga L., 2018, MNRAS, 478, 867
- Pelisoli I., Bell, K., Kepler S. O., Koester D., Romero A. D., 2019, MNRAS, 482, 3831
- Pelisoli I., Vos, J., 2019, MNRAS, 488, 2892
- Pelletier C., Fontaine G., Wesemael F., Michaud G., Wegner G., 1986, ApJ, 307, 242
- Pietrzynski G., Thompson I. B., Gieren W. et al. 2012, Nature, 484, 75
- Schatzman E. L., 1958, White Dwarfs, whdw.book
- Scholz R.-D., Heber U., Heuser C., Ziegerer E., Geier S., Niederhofer F., 2015, A&A, 574, A96
- Sun M., Arras P., 2018, ApJ, 858, 14
- Toonen S., Hollands M., Gänsicke B. T., Boekholt T., 2017, A&A, 602, A16
- Tremblay P-E., Ludwig H.-G., Steffen M., Freytag B., 2013, A&A, 559, A104
- Tremblay P-E., Kalirai J. S., Soderblom D. R., Cignoni M., Cummings J., 2014, ApJ, 791, 92
- Tremblay P-E., Cukanovaite E., Gentile Fusillo N. P., Cunningham T., Hollands M. A., 2019, MNRAS, 482, 5222
- Tremblay P-E., Hollands M. A., Gentile Fusillo N. P., McCleery J., Izquierdo P., Gänsicke B. T., Cukanovaite E., et al., 2020, MNRAS, 497, 130. doi:10.1093/mnras/staa1892
- Whitehouse . J., Farihi J., Green P. J., Wilson T. G., Subasavage J. P., 2018, MNRAS, in press (arXiv:1806.06074)
- Williams B. F., Hillis T. J., Murphy J. W., Gilbert K., Dalcanton J. J., Dolphin A. E., 2018, ApJ, 860, 39. doi:10.3847/1538-4357/aaba7d
- Winget D. E. et al., 1987, ApJ, 315, L77–L81
- Williams K. A., Kepler S. O., Sion E. M., 2019, RNAAS, 3, 109. doi:10.3847/2515-5172/ab3469
- Woosley S. E., Heger A., 2015, ApJ, 810, 34
- Zuckerman B., Koester D., Reid I. N., Hünsch M., 2003, ApJ, 596, 477

This paper has been typeset from a TeX/LaTeX file prepared by the author.

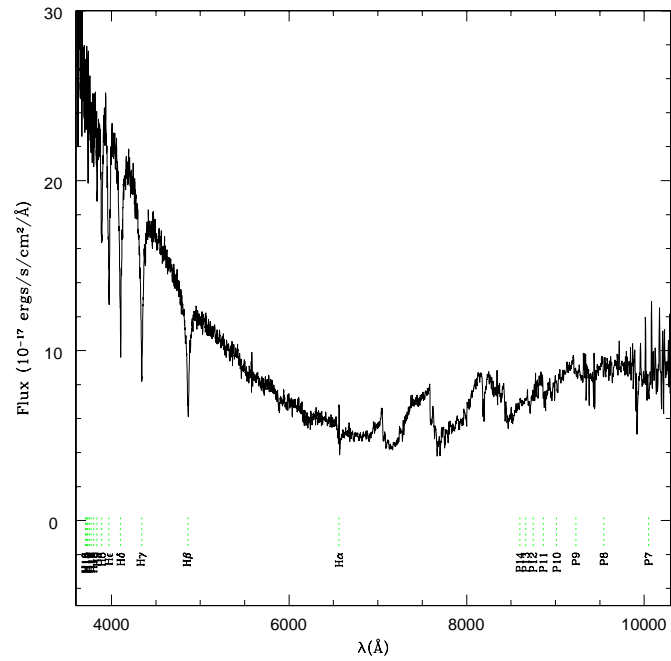
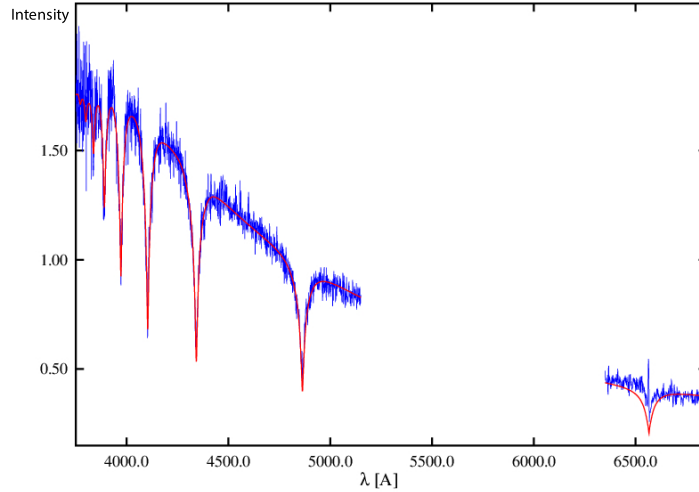


Figure 6. DA+M SDSSJ001626.39+104214.92, $g=18.882$, P-M-F=11565-58507-0320 spectrum in blue and best fitting DA model with $T_{\text{eff}} = 23586 \pm 272$ K, $\log g = 7.561 \pm 0.037$ in red. H α shows contamination from the M unresolved companion, and was not included in the fit. The bottom curve shows the whole SDSS spectrum.

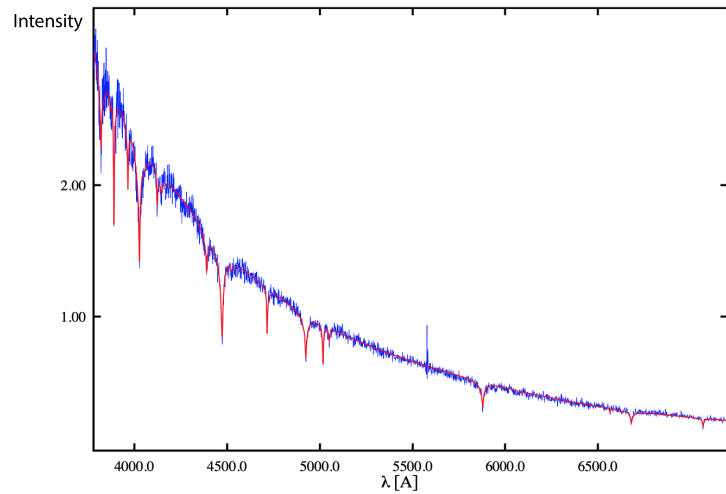


Figure 7. DB SDSS J165222.17+322214.06, $g=17.767$, P-M-F=10909-58280-0663 spectrum in blue and best fitting DB model with $T_{\text{eff}} = 16343 \pm 46$ K, $\log g = 8.126 \pm 0.032$ in red.

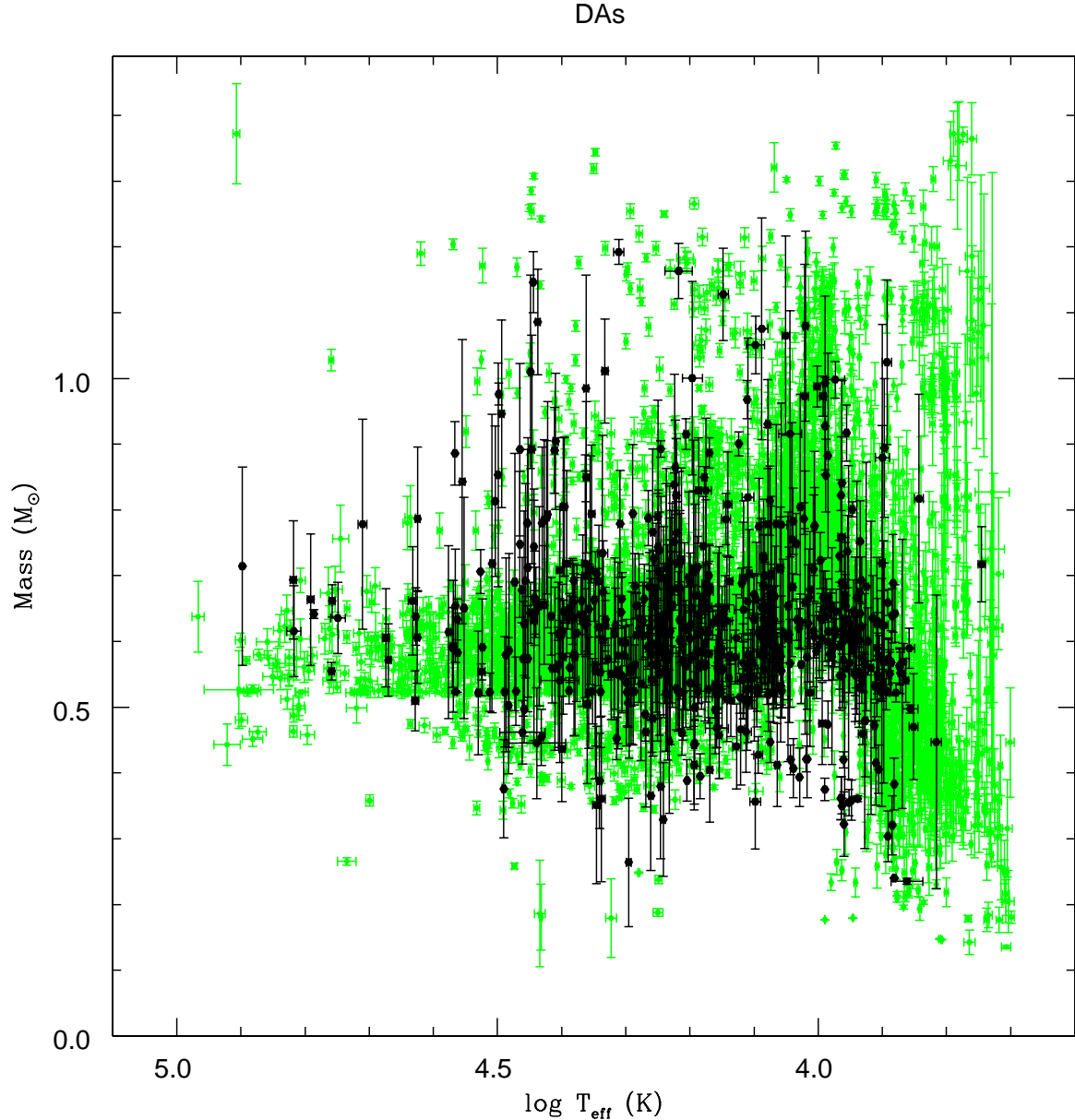


Figure 8. Masses for the 595 best DAs, estimated from the spectroscopic/distances parameters. In the background, we plot the 5951 pure DAs with $S/N_g \geq 15$ from [Kepler et al. \(2019\)](#), corrected to 3D.

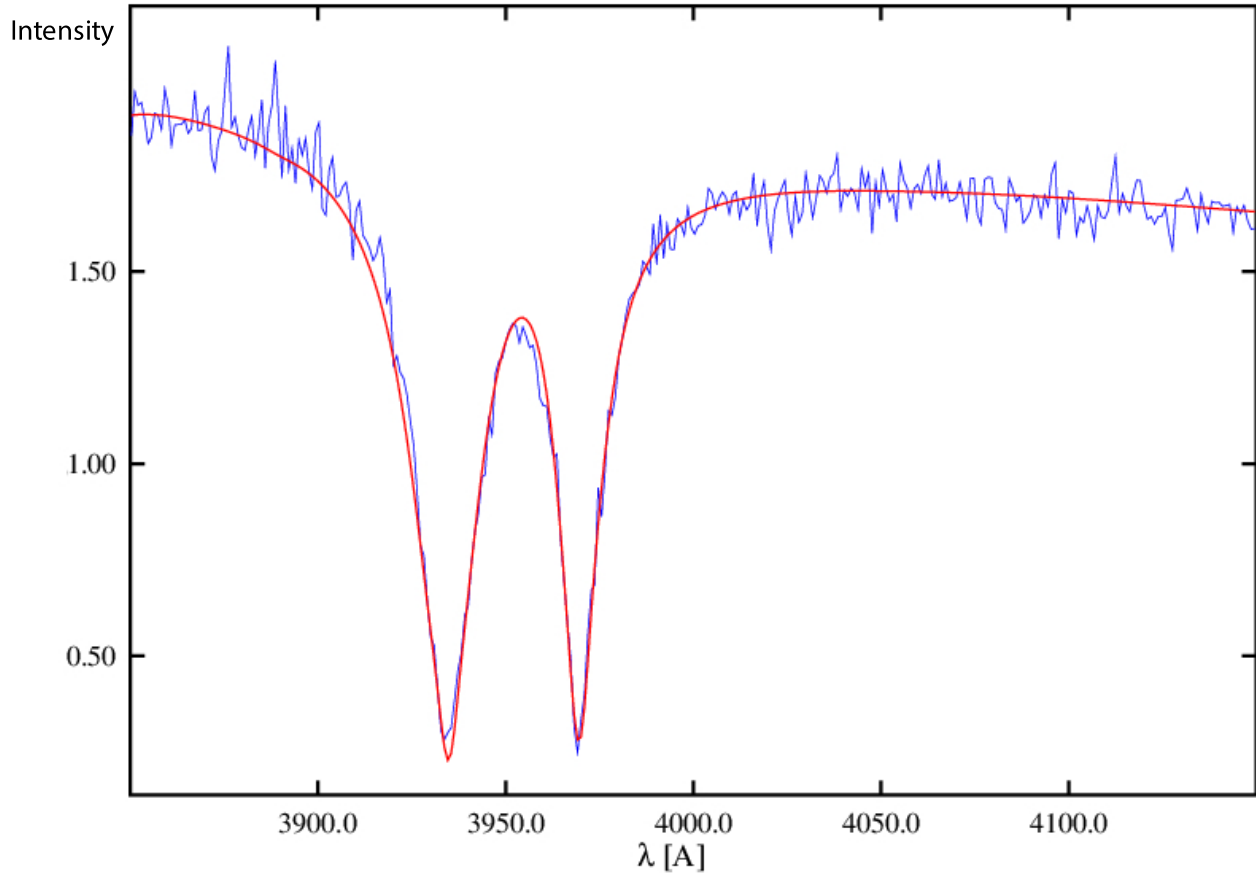


Figure 9. DZ SDSS J131336.95+573800.5, $g=16.895$, P-M-F=1319-52791-0409 in blue, and in red the best model fit at $T_{\text{eff}} = 8695 \pm 90$ K, $\log g = 7.987 \pm 0.022$, $[\text{Ca}/\text{He}] = -9.194 \pm 0.010$, mass = $0.559 \pm 0.009 M_{\odot}$.

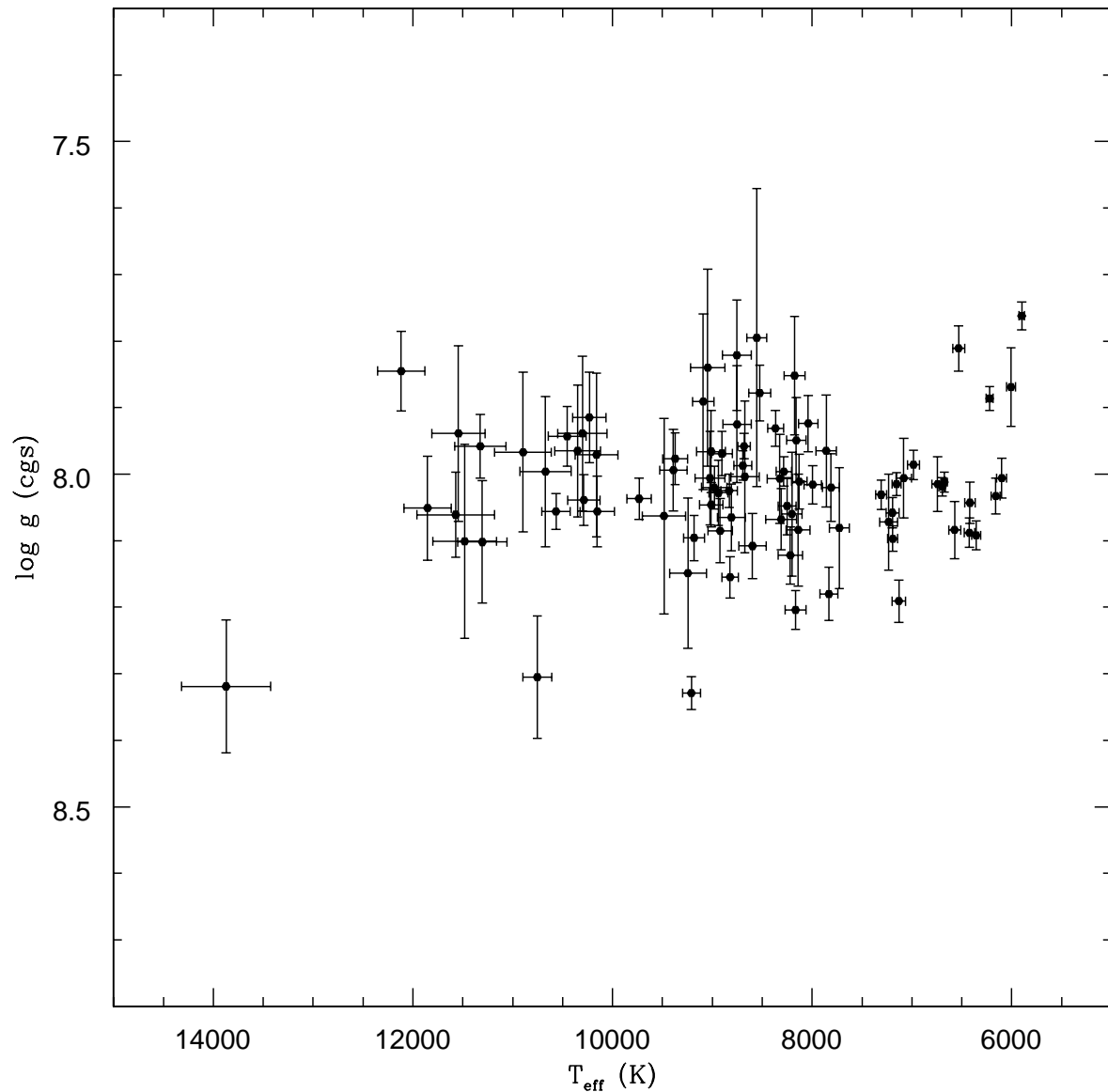


Figure 10. Atmospheric parameters for 85 DZs with $S/N_g \geq 20$ and Gaia parallaxes.

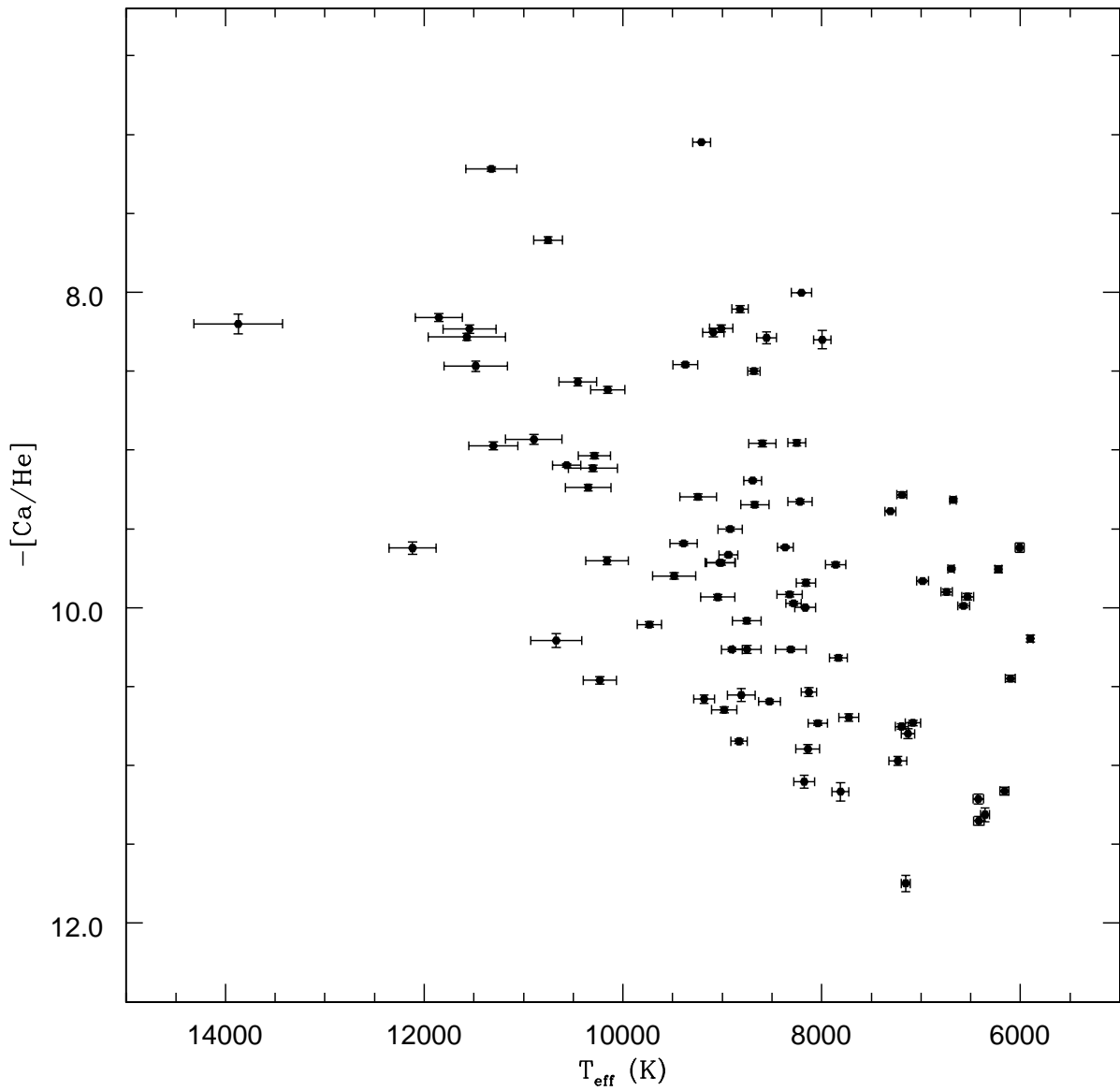


Figure 11. Ca determinations for the sample of $S/N_g \geq 20$ DZs.